L·GARDE
SMART SPACE TECHNOLOGY

L • GARDE INC. CORPORATE PRESENTATION

Analysis of Rim Supports for Off-Axis Inflatable Reflectors I: Loads

Gershon Grossman

Analysis of Rim Supports for Off-Axis Inflatable Reflectors. I: Loads

By Gershon Grossman[1]

Abstract: A structural analysis is performed for the rim support of a pressurized off-axis paraboloidal membrane, serving as a space-based solar concentrator. The function of the rim support is to take up the tensile forces created by the stretched membrane. This paper deals with the load analysis. The tensile forces transmitted by the membrane to the rim support are calculated, and are proportional to pb, where p is the inflation pressure and b is one-half the major axis of the elliptical rim. Next, the internal forces and moments generated in the rim support by the membrane forces are calculated. The compression forces are considerably larger, at any point, than the shear forces; both are proportional to pb^2. The bending moments are proportional to pb^3. The critical point is found to be at the top of the rim, where both the bending moment and compression force are at their maximum.

Introduction

Inflatable structures employing thin, pressurized membranes almost invariably require some form of rim support (Arduini et al. 1988; Kato et al. 1988; Belvin et al. 1987; Hedgepeth 1985). The application to solar reflectors or pressurized antennas, for example, requires the membrane to assume a paraboloidal shape of considerable accuracy; the inflation pressure must be large enough to provide a smooth surface and eliminate any wrinkles or waviness (Thomas and Friese 1980). The pressure acting over the membrane surface creates a sizable force that must be taken up by the rim support at the edges of the membrane. The rim support must have not only the strength to carry this load, but also the rigidity to resist deformation and allow the membrane to maintain its accurate shape.

The purpose of the present analysis has been to calculate the loads on the rim support of the deployable solar concentrator (Grossman and Williams 1989), which carries two geometrically identical membranes, one serving as a reflector and the other as a canopy, in an off-axis paraboloidal configuration. The rim support contemplated for this unit is an elliptical torus with a circular cross section. In this study we prefer to employ the more general term *rim support* rather than *torus* since the toroidal shape is a particular case and is not necessarily the optimal one for supporting the membranes.

The forces transmitted to the rim support by the membranes create in it internal compression and shear forces as well as bending moments. To design the rim support, one must calculate these loads and the stresses resulting from them, as well as the deformations they generate. This paper describes the method of analysis and the expressions developed for the loads. The scaling parameters of the system are derived in terms of the membrane ge-

[1]Prof., Dept. of Mech. Engrg., Technion, Israel Inst. of Tech., 32000 Haifa, Israel; formerly Program Engr., L'Garde, Inc., 15181 Woodlawn Ave., Tustin, CA 02680.

Note. Discussion open until June 1, 1991. Separate discussions should be submitted for the individual papers in this symposium. To extend the closing date one month, a written request must be filed with the ASCE Manager of Journals. The manuscript for this paper was submitted for review and possible publication on April 27, 1989. This paper is part of the ***Journal of Aerospace Engineering***, Vol. 4, No. 1, January, 1991. ©ASCE, ISSN 0893-1321/91/0001-0047/$1.00 + $.15 per page. Paper No. 25373.

ometry and inflation pressure. A companion paper describes the deformation analysis.

Forces in Paraboloidal Membrane

The first step toward the evaluation of the rim support loads is to calculate the tension forces in the membrane. The geometry of the off-axis membrane is quite complex; the calculation may be simplified because this membrane forms part of a larger, axisymmetrical paraboloid. The geometry of the uninflated off-axis membrane and the gore and mandrel shapes used in its fabrication are all calculated based on this (Williams 1987).

Fig. 1 describes the geometry of the off-axis paraboloidal membrane and the forces it applies at points along the rim. The off-axis shape is formed by a plane intersecting the parent paraboloid of revolution

$$z = \frac{r^2}{4F} \quad \ldots\ldots (1)$$

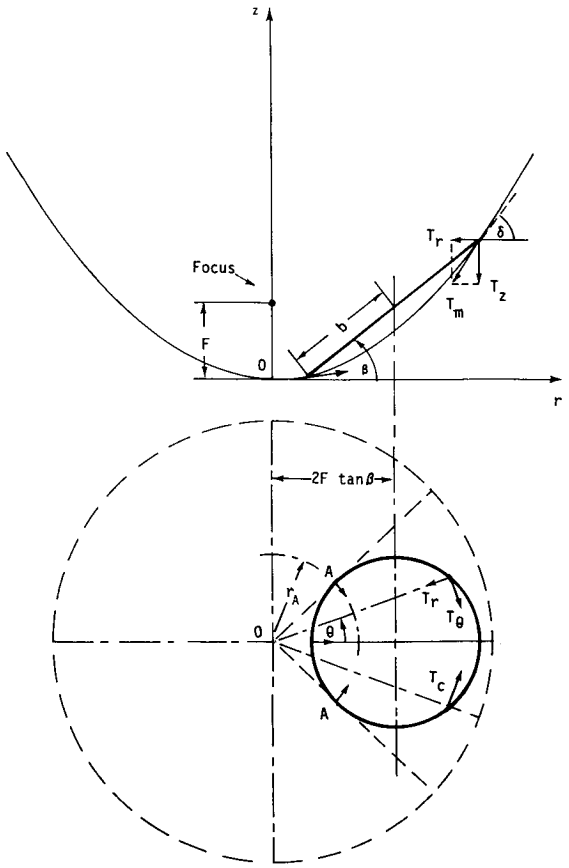

FIG. 1. Geometry of Off-Axis Paraboloidal Membrane

at angle β. The rim is an ellipse with the major and minor axes $2b$ and $2b \cos \beta$, respectively. When viewed along the paraboloid's axis, the rim assumes the shape of a circle with a diameter equal to the ellipse's minor axis and a center at distance $2F \tan \beta$ from the paraboloid's axis. Note that the parameters F, b, and β determine the geometry of the off-axis membrane completely and uniquely.

The principal stresses in a thin-walled body of revolution may be calculated readily based on the internal pressure and the radii of curvature in the meridional and circumferential directions (Roark 1971). In this analysis of the membrane it is convenient to consider the tensile forces per unit length, which are equal, at each point, to the stress times the thickness. The principal tensile forces in the on-axis paraboloid, T_m in the meridional direction and T_c in the circumferential direction, are shown in Fig. 1. T_m at a particular height z may be calculated by cutting the paraboloid perpendicular to its axis and equating the z-component of the meridional force operating along the cut edge with the pressure force in the opposite direction

$$2\pi r T_m \sin \delta = \pi r^2 p \quad \ldots\ldots (2)$$

Then, T_c may be found from its relation to T_m, the pressure and the radii of curvature R_m and R_c in the meridional and circumferential directions, respectively (Roark 1971)

$$p = \frac{T_m}{T_m} + \frac{T_c}{R_c} \quad \ldots\ldots (3)$$

Calculating the geometrical parameters from the paraboloid of Eq. 1, we find

$$\tan \delta = \frac{dz}{dr} = \frac{r}{2F} \quad \ldots\ldots (4)$$

$$R_c = \frac{r}{\sin \delta} = 2F\left[1 + \left(\frac{r}{2F}\right)^2\right]^{1/2} \quad \ldots\ldots (5)$$

$$R_m = \frac{\left[1 + \left(\frac{dz}{dr}\right)^2\right]^{3/2}}{\frac{d^2z}{dr^2}} = 2F\left[1 + \left(\frac{r}{2F}\right)^2\right]^{3/2} \quad \ldots\ldots (6)$$

Substitution in Eqs. 2 and 3 yields

$$T_m = pF\left[1 + \left(\frac{r}{2F}\right)^2\right]^{1/2} \quad \ldots\ldots (7)$$

$$T_c = pF \frac{1 + 2\left(\frac{r}{2F}\right)^2}{\left[1 + \left(\frac{r}{2F}\right)^2\right]^{1/2}} \quad \ldots\ldots (8)$$

Forces Transmitted to Rim Support

The tensile forces in the on-axis paraboloid are now applied along the elliptical rim forming the edge of the off-axis membrane. Fig. 2(*a*) describes the rim on a Cartesian coordinate system with its origin at the center of the ellipse, with x, y, and n along the minor axis, the major axis, and normal to the ellipse's plane, respectively. Consider a small element of the rim of length dl, with a small portion of membrane attached to it, cut along one meridional and one circumferential line. As illustrated in Fig. 2(*b*), the meridional tensile force T_m operates along a cut edge of length dS_c and the circumferential tensile force T_c operates along a cut edge of length dS_m. The membrane forces to be taken up by the rim support are therefore $T_c dS_m$ in the circumferential direction, $T_m dS_c$ in the meridional direction, and $pdS_c dS_m/2$ normal to the membrane. Note that the pressure force is an order of magnitude smaller than the two others, as it includes a product of two differentials, and vanishes in the limit.

The membrane forces are counterbalanced by rim forces, operating along the membrane/rim support boundary of length dl, as follows: $T_x dl$ in the x-direction, $T_y dl$ in the y-direction, and $T_n dl$ in the n-direction. Force balances on the element of Fig. 2(*b*) in the x-, y-, and n-directions yield T_x, T_y, and T_n from the known T_c and T_m.

Because of the complex geometrical relations governing the conversion of various vectors from the membrane coordinates along meridional and circumferential directions to those in the plane of the rim, it is convenient to carry out the conversion in two steps. First, the membrane forces and length elements are expressed in terms of their components along the axes r, θ, and z of a cylindrical coordinate system as shown in Fig. 1. Next, the change from the cylindrical to the rim coordinate system is executed.

In the cylindrical coordinate system

$$dS_m = \sqrt{dr^2 + dz^2} = \left[1 + \left(\frac{r}{2F}\right)^2\right]^{1/2} dr \quad \ldots\ldots (9a)$$

$$dS_c = r d\theta \quad \ldots\ldots (9b)$$

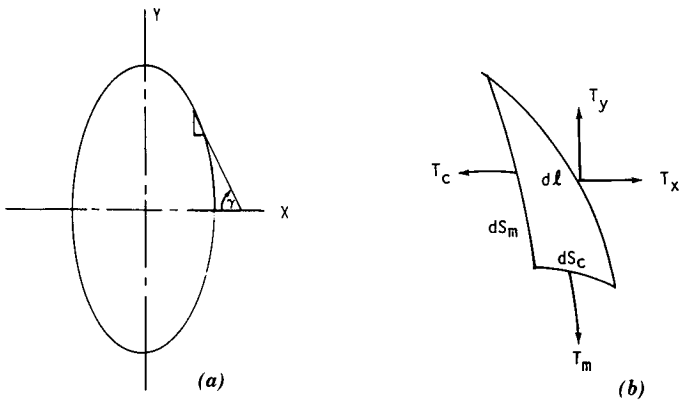

FIG. 2. Forces Transmitted to Rim Support by Pressurized Membrane: (*a*) Membrane Element Location; and (*b*) Forces Applied to Membrane Element

The meridional force T_m is broken into axial and radial components, T_z and T_r, as shown in Fig. 1. The circumferential force T_c is in the same direction as $T\theta$. (Note that the sign has to be matched when switching from the membrane to the cylindrical coordinate system. T_r, T_z and $T\theta$ shown at the top part of the rim in Fig. 1 are all in the negative directions.) Using the slope angle δ of the on-axis paraboloid, Eq. 4, and the expressions for T_c and T_m (Eqs. 7 and 8), we can calculate the total membrane forces transmitted to the rim element dl in the radial, circumferential, and axial directions as follows:

$$T_r dS_c = T_m \cos\delta dS_c = pFrd\theta \quad \ldots\ldots (10a)$$

$$T_\theta dS_m = T_c dS_m = pF\left[1 + 2\left(\frac{r}{2F}\right)^2\right]dr \quad \ldots\ldots (10b)$$

$$T_z dS_c = T_m \sin\delta dS_c = p\frac{r^2}{2}d\theta \quad \ldots\ldots (10c)$$

Figs. 1 and 2 help illustrate the conversion from the cylindrical to the rim coordinate system. Starting with the axial component T_z, we notice that it forms a fixed angle β with the n-axis, perpendicular to the ellipse's plane, at all points along the rim. It contributes components only in the y- and n-directions, $T_z \sin\beta$ and $T_z \cos\beta$, respectively, and none in the x-direction. T_r and $T\theta$, best illustrated on the bottom part of Fig. 1, may each be broken into an x-component and another one perpendicular to it in the r-θ plane, which is broken further into y- and n-components. Taking this into consideration and writing a force balance in the x-, y-, and n-directions, we obtain

$$T_x dl = (T_r dS_c)\sin\theta + (T_\theta dS_m)\cos\theta \quad \ldots\ldots (11a)$$

$$T_y dl = (T_r dS_c)\cos\theta\cos\beta - (T_\theta dS_m)\sin\theta\cos\beta + (T_z dS_c)\sin\beta \quad \ldots\ldots (11b)$$

$$T_n dl = -(T_r dS_c)\cos\theta\sin\beta + (T_\theta dS_m)\sin\theta\sin\beta + (T_z dS_c)\cos\beta \quad \ldots\ldots (11c)$$

where

$$\theta = \sin^{-1}\frac{x}{r} \quad \ldots\ldots (12)$$

as is evident from Fig. 2.

Substitution in Eqs. 11*a*–*c* from Eqs. 10*a*–*c* yields

$$T_x = pF\left\{x\frac{d\theta}{dl} + \left[1 + 2\left(\frac{r}{2F}\right)^2\right]\sqrt{1 - \left(\frac{x}{r}\right)^2}\frac{dr}{dl}\right\} \quad \ldots\ldots (13a)$$

$$T_y = pF\left\{\left[\sqrt{r^2 - x^2}\cos\beta + \frac{r^2}{2F}\sin\beta\right]\frac{d\theta}{dl} - \left[1 + 2\left(\frac{r}{2F}\right)^2\right]\frac{x}{r}\cos\beta\frac{dr}{dl}\right\} \quad \ldots\ldots (13b)$$

$$T_n = pF\left\{\left[\frac{r^2}{2F}\cos\beta - \sqrt{r^2 - x^2}\sin\beta\right]\frac{d\theta}{dl}\right.$$

[*Continued*]

$$+\left[1+2\left(\frac{r}{2F}\right)^2\right]\frac{x}{r}\sin\beta\,\frac{dr}{dl}\Bigg\} \quad \ldots\ldots (13c)$$

To complete the conversion, it is necessary to express r, dr/dl, and $d\theta/dl$, in Eqs. 13a–c in terms of the rim coordinates, x and y. First, we note that

$$dl^2 = dS_c^2 + dS_m^2 = dx^2 + dy^2 \quad \ldots\ldots (14)$$

x and y are related to each other by the ellipse's equation

$$\frac{x^2}{b^2\cos^2\beta} + \frac{y^2}{b^2} = 1 \quad \ldots\ldots (15)$$

so that

$$x = \sqrt{b^2 - y^2}\cos\beta \qquad dx = -\frac{y\cos\beta}{\sqrt{b^2 - y^2}}\,dy \quad \ldots\ldots (16)$$

and

$$dl = \sqrt{dx^2 + dy^2} = \sqrt{\frac{b^2 - y^2\sin^2\beta}{b^2 - y^2}}\,dy \quad \ldots\ldots (17)$$

The relation of r to x and y is found from geometrical considerations

$$r^2 = x^2 + (2F\tan\beta + y\cos\beta)^2 \quad \ldots\ldots (18)$$

Substituting x from Eq. 16 we obtain

$$r^2 = 4F^2\tan^2\beta + b^2\cos^2\beta + 4Fy\sin\beta \quad \ldots\ldots (19)$$

Also, at each point on the ellipse, lying on a plane inclined at angle β

$$dz = \sin\beta\,dy \quad \ldots\ldots (20)$$

and therefore, from Eq. 4

$$dr = \frac{2F}{r}\,dz = \frac{2F\sin\beta}{r}\,dy \quad \ldots\ldots (21)$$

Substituting from Eq. 11 in Eq. 14 we obtain

$$rd\theta = \sqrt{dl^2 - dr^2 - dz^2} = \left[\frac{b^2\cos^2\beta}{b^2 - y^2} - \frac{\sin^2\beta}{\left(\frac{r}{2}F\right)^2}\right]^{1/2} dy \quad \ldots\ldots (22)$$

We have now expressed all the differentials in terms of dy and may find the derivatives dr/dl and $d\theta/dl$ from Eqs. 17, 21, and 22.

$$\frac{dr}{dl} = \frac{2F\sin\beta}{r}\sqrt{\frac{b^2 - y^2}{b^2 - y^2\sin^2\beta}} \quad \ldots\ldots (23)$$

$$\frac{d\theta}{dl} = \pm\frac{1}{r}\left[\frac{b^2}{(b^2 - y^2)\tan^2\beta} - \left(\frac{2F}{r}\right)^2\right]^{1/2}\sin\beta\sqrt{\frac{b^2 - y^2}{b^2 - y^2\sin^2\beta}} \quad \ldots\ldots (24)$$

The $\pm$ sign in Eq. 24 accounts for $d\theta/dl$ changing sign at points A along

the rim (Fig. 1), when proceeding in the positive y-direction, from a positive value for points characterized by $r < r_A$ to a negative value for points characterized by $r > r_A$. A marks the point where the meridian is tangent to the rim. Note that $d\theta/dl$ appears in the terms originating from T_r and T_z in Eqs. 13a–c. We notice that $T\theta$ always operates on the rim in the negative θ-direction. However, T_r and T_z, both components of T_m, switch sign at the points A. The part of the rim characterized by $r < r_A$ sees T_r and T_z acting on it in the positive r- and z-directions. The reverse is true for the part of the rim characterized by $r > r_A$. r_A at the tangent point may be readily found from geometrical considerations

$$r_A = \sqrt{(2F\tan\beta)^2 - (b\cos\beta)^2} \quad \ldots\ldots (25)$$

It is easily verified that for $r = r_A$, $d\theta/dl$ in Eq. 24 vanishes.

Finally, substitution of x, r, dr/dl, and $d\theta/dl$ from Eqs. 16, 23, and 24 into Eqs. 13a–c will yield the forces exerted on the rim, T_x, T_y, and T_n, per unit length of rim, for each y. The expressions may be written in the following dimensionless form:

$$T_x = (pb)T_x^*, \qquad T_y = (pb)T_y^*, \qquad T_m = (pb)T_m^* \quad \ldots\ldots (26)$$

where T_x^*, T_y^*, and T_n^* = dimensionless functions of β and of

$$F_1 = \frac{F}{b}, \qquad y_1 = \frac{y}{b} \quad \ldots\ldots (27)$$

as follows:

$$T_x^* = [\pm CD + \sqrt{1 - C^2}(1 + 2B^2)]\frac{F_1\sin\beta}{BK} \quad \ldots\ldots (28a)$$

$$T_y^* = [\pm(\sqrt{1 - C^2}\cos\beta + B\sin\beta)D - (1 + 2B^2)C\cos\beta]\frac{F_1\sin\beta}{BK} \quad \ldots (28b)$$

$$T_n^* = [\pm(B\cos\beta - \sqrt{1 - C^2}\sin\beta)D + (1 + 2B^2)C\sin\beta]\frac{F_1\sin\beta}{BK} \quad \ldots (28c)$$

where

$$B = \sqrt{\tan^2\beta + \frac{\cos^2\beta}{4F_1^2} + \frac{y_1}{F_1}\sin\beta} \quad \ldots\ldots (29)$$

$$C = \frac{\sqrt{1 - y_1^2}\cos\beta}{2F_1B} \quad \ldots\ldots (30)$$

$$D = \sqrt{\frac{B^2}{(1 - y_1^2)\tan^2\beta} - 1} \quad \ldots\ldots (31)$$

$$K = \sqrt{\frac{1 - y_1^2\sin^2\beta}{1 - y_1^2}} \quad \ldots\ldots (32)$$

Note that the scaling factor pb applies to all the tensile forces per unit length of rim, T_x, T_y, and T_n, transmitted to the rim by the membrane.

Fig. 3 describes the distribution of T_x and T_y along the elliptical rim, for

Internal Forces and Moments in Rim Support

Having calculated the tensile forces exerted by the membrane on the rim support, we can calculate the internal reactions—forces and moments—produced in it by the external load. These internal forces and moments result in stresses in the rim support material, which must be determined to calculate the strength. We will employ the free-body method, where the rim support is cut and a portion of it, subject to external loading, is analyzed.

Taking advantage of the symmetry with respect to the y-axis, we choose to make the first cut along the axis, as illustrated in Fig. 5(a). The reactions at the two cut ends are marked by F_L and M_L at the low end (closest to the paraboloid's axis) and F_H and M_H at the high end (farthest from the paraboloid's axis). Symmetry does not allow any shear forces in the y-direction because of the requirement for them to be equal and opposite on the two sides of the section. Consequently, there are only forces normal to the cross section (i.e., in the x-direction) and bending moments, as shown. Force balances on the right half of the rim support in the x- and y-directions yield

$$\Sigma P_x = F_L + F_H + \int_{y=-b}^{+b} T_x dl = 0 \quad \ldots\ldots (36)$$

$$\Sigma P_y = \int_{y=-b}^{+b} T_y dl = 0 \quad \ldots\ldots (37)$$

A moment balance about the low cut end gives

$$\Sigma M = M_L + M_H - 2bF_H + \int_{y=-b}^{+b} xT_y dl - \int_{y=-b}^{+b} (y + b)T_x dl = 0 \quad \ldots\ldots (38)$$

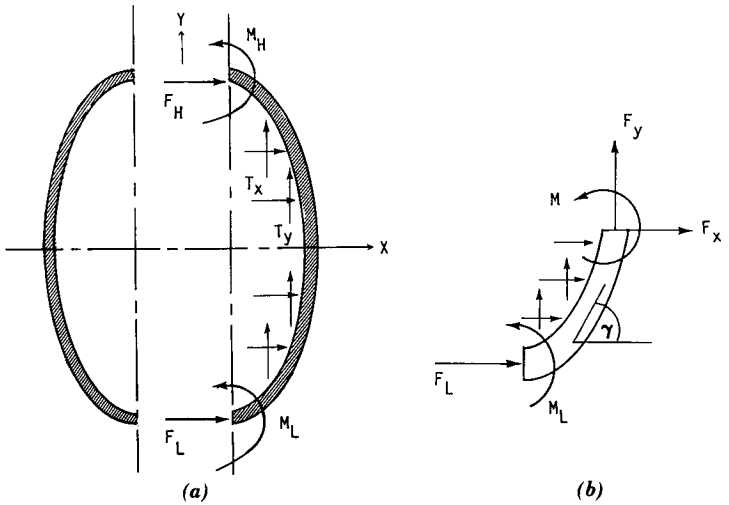

FIG. 5. Internal Forces and Moments in Rim Support: (*a*) Cut along Axis of Symmetry; and (*b*) Loads Applied to Rim Element

Eq. 37 does not provide any new information, since it does not contain any of the reactions. It merely provides a check on T_y that was calculated earlier, to confirm that y tensile forces on the rim are balanced. We thus have two equations, Eqs. 36 and 38, for the four unknowns, F_L, F_H, M_L, and M_H. The problem is clearly statically indeterminate.

Additional information on this type of problem must be obtained from an analysis of the deformations. In this particular example, due to the symmetry with respect to the y-axis, it is required that the horizontal deflections as well as the angular deformations at the cut ends by zero. There are several ways of implementing this requirement to calculate the reactions, including virtual work and the like. We will employ Castigliano's second theorem (Marim and Sauer 1954), which makes use of the strain energy U. This energy is calculated in terms of the unknown reactions. To obtain the two additional equations required to solve the present problem, we express U in terms of M_L and F_L and require that

$$\frac{\partial U}{\partial M_L} = 0 \quad \ldots\ldots (39)$$

$$\frac{\partial U}{\partial F_L} = 0 \quad \ldots\ldots (40)$$

The total strain energy contains terms associated with tension/compression, shear, and bending of the rim support. To calculate it, we must find the normal and tangential forces and the bending moments at each cross section. To this end, we cut the right half of the rim support further, at an arbitrary point, as shown in Fig. 5(b). We load the cut end with internal forces F_x and F_y and with a bending moment M, as shown. A force balance in the x- and y-directions and a sum of moments about the low cut end give three equations for F_x, F_y, and M in terms of the two still unknown reactions F_L and M_L

$$\Sigma P_x = F_L + F_x + \int_{y=-b}^{y} T_x dl = 0 \quad \ldots\ldots (41)$$

$$\Sigma P_y = F_y + \int_{y=-b}^{y} T_x dl = 0 \quad \ldots\ldots (42)$$

$$\Sigma M = M_L + M - (y + b)F_x + xF_y - \int_{y=-b}^{y} (y + b)T_x dl$$

$$+ \int_{y=-b}^{y} xT_y dl = 0 \quad \ldots\ldots (43)$$

Substituting T_x and T_y from Eq. 26, dl from Eq. 17, and solving, we find

$$F_x(y) = -F_L - pb^2 \int_{-1}^{y_1} T_x^* K dy_2 \quad \ldots\ldots (44)$$

$$F_y(y) = -pb^2 \int_{-1}^{y_1} T_y^* K dy_2 \quad \ldots\ldots (45)$$

$$M(y) = -M_L - (1 + y_1)bF_L - (1 + y_1)(pb^3)\int_{-1}^{y_1} T_x^* K dy_2$$

$$+ \sqrt{1 - y_1^2}\cos\beta\,(pb^3)\int_{-1}^{y_1} T_y^* K dy_2 + (pb^3)\int_{-1}^{y_1}(1 + y_2)T_x^* K dy_2$$

$$- \cos\beta\,(pb^3)\int_{-1}^{y_1}\sqrt{1 - y_2^2}\,T_y^* K dy_2 \quad \ldots\ldots (46)$$

where $y_1 = y/b$, Eq. 27, and y_2 = a variable of integration to be substituted for y_1 in the expressions for T_x^*, T_y^*, and K, In particular, for $y = b$, $F_x = F_H$, $F_y = 0$, $M = M_H$ as may be verified by comparing Eqs. 44–46 with Eqs. 36–38.

The form of Eqs. 44–48 yields the scaling laws for the internal forces and moments. It is evident that the forces scale with pb^2 and the moments with pb^3. Using the normalized quantities

$$F_x^* = \frac{F_x}{(pb^2)} \quad \ldots\ldots (47a)$$

$$F_y^* = \frac{F_y}{(pb^2)} \quad \ldots\ldots (47b)$$

$$F_L^* = \frac{F_L}{(pb^2)} \quad \ldots\ldots (47c)$$

$$F_H^* = \frac{F_H}{(pb^2)} \quad \ldots\ldots (47d)$$

$$M^* = \frac{M}{(pb^3)} \quad \ldots\ldots (47e)$$

$$M_L^* = \frac{M_L}{(pb^3)} \quad \ldots\ldots (47f)$$

$$M_H^* = \frac{M_H}{(pb^3)} \quad \ldots\ldots (47g)$$

Eqs. 44–46 may be rewritten in a completely dimensionless form.

From F_x and F_y we may calculate the shear forces (normal to the ellipse) and the tension/compression forces (tangential to the ellipse), F_S and F_T, respectively, at each cross section, as follows:

$$F_T = F_y \sin\gamma - F_x \cos\gamma \quad \ldots\ldots (48a)$$

$$F_S = F_y \cos\gamma + F_x \sin\gamma \quad \ldots\ldots (48b)$$

Or in normalized form

$$F_T^* = \frac{F_T}{(pb^2)}, \qquad F_S^* = \frac{F_S}{(pb^2)} \quad \ldots\ldots (49)$$

With F_S, F_T, and M known at points along the rim, the total strain energy may be found from the formula (Popov 1952)

$$U = \oint\left(\frac{M^2}{2EI} + \frac{F_T^2}{2EA} + \frac{sF_s^2}{2GA}\right)dl \quad \ldots\ldots (50)$$

where the three terms from left to right represent energy associated with bending, tension/compression, and shear, respectively; E and G = the modulii of elasticity and shear, respectively, of the rim support material; A = the cross-section area; and I = the moment of inertia of the cross section for bending about an axis normal to the x-y plane. The dimensionless factor, s, expresses that the shear stresses are not uniformly distributed over the cross section area; its value depends on the shape of the cross section. We will see later that the shear forces are considerably smaller than the tension/compression forces for typical off-axis geometries; they vanish completely in the rim support of an on-axis membrane. Hence, the shear energy is small compared to the tension/compression energy, and both are generally small compared to the energy due to bending.

Eq. 52 may be rewritten in a dimensionless form, by substituting the normalized quantities from Eqs. 47 and 49 as follows:

$$U = \frac{p^2b^7}{EI}\int_{-1}^{+1}(M^{*2} + iF_T^{*2} + jF_S^{*2})K dy_1 \quad \ldots\ldots (51)$$

where i and j = dimensionless parameters

$$i = \frac{I}{Ab^2} \quad \ldots\ldots (52)$$

$$j = s\frac{EI}{GAb^2} \quad \ldots\ldots (53)$$

and are generally much smaller than unity.

F_T^* and F_S^* in Eq. 51 are functions of the still unknown F_L; M^* is a function of both F_L and M_L. Substitution in Eqs. 39 and 40 yields

$$\int_{-1}^{+1} M^*\frac{\partial M^*}{\partial M_L^*}K dy_1 = 0 \quad \ldots\ldots (54)$$

$$\int_{-1}^{+1}\left(M^*\frac{\partial M^*}{\partial F_L^*} + iF_T^*\frac{\partial F_T^*}{\partial F_L^*} + jF_S^*\frac{\partial F_S^*}{\partial F_L^*}\right)K dy_1 = 0 \quad \ldots\ldots (55)$$

Using Eqs. 48a–b and 50 to express F_T^* and F_S^* in terms of F_x^* and F_y^* and calculating the derivatives from Eqs. 44–46, we find

$$\frac{\partial M^*}{\partial M_L^*} = -1 \quad \ldots\ldots (56a)$$

$$\frac{\partial M^*}{\partial F_L^*} = -(1 + y_1) \quad \ldots\ldots (56b)$$

$$\frac{\partial F_T^*}{\partial F_L^*} = \cos\gamma \quad \ldots\ldots (56c)$$

$$\frac{\partial F_S^*}{\partial F_L^*} = -\sin\gamma \quad \text{(56}d\text{)}$$

and hence, Eqs. 56 and 57 become

$$\int_{-1}^{+1} M^* K dy_1 = 0 \quad \text{(57)}$$

$$\int_{-1}^{+1} [(1 + y_1)M^* - i\cos\gamma F_T^* + j\sin\gamma F_S^*]K dy_1 = 0 \quad \text{(58)}$$

Let

$$H_1(y_1) = \sqrt{1 - y_1^2}\cos\beta \int_{-1}^{y_1} T_y^* K dy_2 - (1 + y_1)\int_{-1}^{y_1} T_x^* K dy_2$$

$$+ \int_{-1}^{y_1} [(1 + y_2)T_x^* - \sqrt{1 - y_2^2}\cos\beta\, T_y^*]K dy_2 \quad \text{(59)}$$

$$H_2(y_1) = i\cos^2\gamma + j\sin^2\gamma)\int_{-1}^{y_1} T_x^* K dy_2 + (j - i)\sin\gamma\cos\gamma\int_{-1}^{y_1} T_y^* K dy_2 \quad \text{(60)}$$

Then, substitution from Eq. 46 in Eq. 57 yields

$$M_L^*\int_{-1}^{+1} K dy_1 + F_L^*\int_{-1}^{+1}(1 + y_1)K dy_1 = \int_{-1}^{+1} H_1 K dy_1 \quad \text{(61)}$$

and substitution from Eqs. 44–46, 48*a*–*b*, and 49 into Eq. 58

$$M_L^*\int_{-1}^{+1}(1 + y_1)K dy_1 + F_L^*\int_{-1}^{+1}[(1 + y_1)^2 + i\cos^2\gamma + j\sin^2\gamma]K dy_1$$

$$= \int_{-1}^{+1}[(1 + y_1)H_1 - H_2]K dy_1 \quad \text{(62)}$$

where $\sin\gamma$ and $\cos\gamma$ in Eqs. 60 and 62 are functions of y_1, as per Eq. 35.

Eqs. 61 and 62, provided by Castigliano's second theorem for this statically indeterminate problem, may be solved for F_L^* and M_L^*, once the integrals are evaluated. We notice that the integrals contain the membrane loads T_x^* and T_y^*, geometrical parameters of the off-axis paraboloid and rim support, and the cross-section parameters i and j—all given or known from earlier calculations. Once the low-end reactions F_L^* and M_L^* are found, we can calculate F_H^* and M_H^* from the equilibrium Eqs. 36 and 38. This completes the problem, since now all the internal forces and moments are given through the expressions already developed, linking them to the low-end reactions.

Results

The integrals in Eqs. 59–62 are elliptic, and cannot be calculated analytically. A computer code based on the foregoing analysis was used to calculate the internal forces and moments in the rim support for the geometry of the deployable solar concentrator (Grossman and Williams 1989). We assume $i = j = 0$, a good assumption for most practical cases, as is evident from Eqs. 52 and 53.

Fig. 6 shows the distribution along the elliptical rim of F_x (on the right) and F_y (on the left). The positive directions of F_x and F_y are indicated in Fig. 5(*b*), as they operate on the top cut end of the portion shown. Thus, F_x at $y = -b$ is equal in magnitude and opposite in direction to F_L. Proceeding upward along the rim (y increases), F_x becomes smaller and smaller as the contribution of membrane forces pulling inward toward balancing off the reaction F_L increases. By the time $y = 0$ is reached, the sum of membrane forces T_x over the bottom half of the rim is approximately equal to F_L, and hence $F_x = 0$. Further up, F_x reverses direction to help F_L in counterbalancing the membrane forces, and at the top ($y = +b$), F_x becomes equal to the top reaction F_H. A similar behavior is exhibited by F_y, which must counterbalance the membrane forces T_y. There are no y reactions, however, at the cut ends, for reasons of symmetry as explained in the previous section. Thus, $F_y = 0$ at $y = -b$, and increases with increasing y, pointing downward, to balance off the membrane forces pulling inward. F_y reaches its maximum at $y = +0.24b$, as shown, and then begins to decrease, as T_y forces pulling inward reverse their direction (Fig. 3). This trend continues until F_y is reduced to zero at $y = +b$.

Fig. 7 describes the internal force distribution from a different angle, where F_x and F_y have been replaced by shear and compression forces, F_S and F_T,

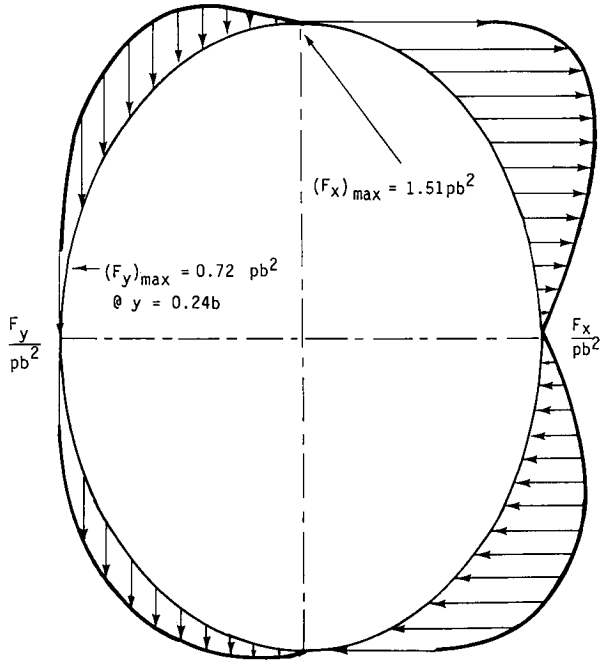

FIG. 6. Distribution along Rim of Internal Forces in *x*- and *y*-Directions

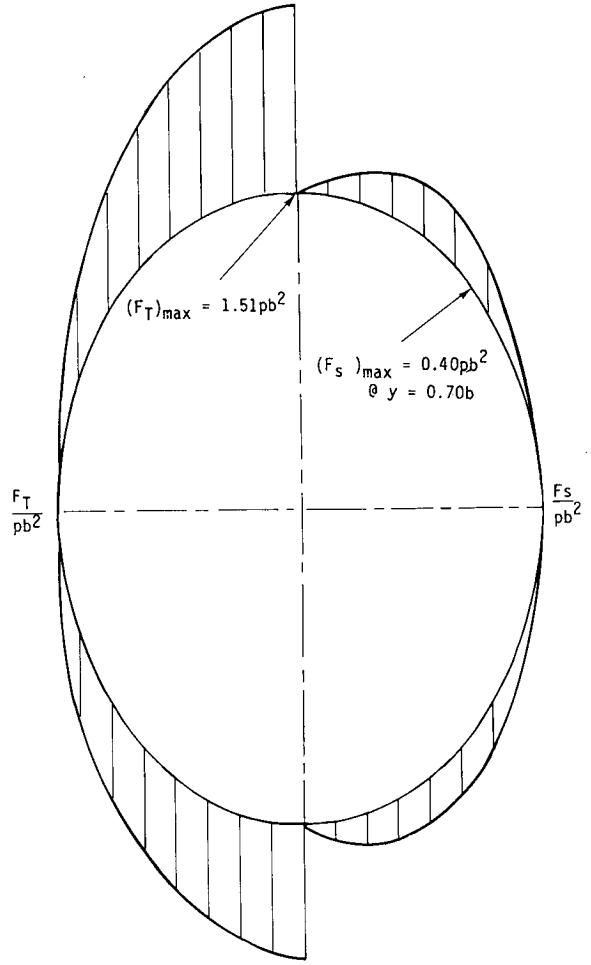

FIG. 7. Distribution along Rim of Internal Forces in Normal and Tangential Directions

respectively, as per Eqs. 48*a–b*. (The distribution along the rim is described in terms of the vertical bars, which indicate magnitude, but not direction.) F_s is shown on the right part of the ellipse and F_T on the left. It is clear that the compression force at each point is considerably greater than the shear force. The maximum compressive load is reached at the top of the rim ($y = +b$) and is approximately $1.5pb^2$.

Fig. 8 describes the distribution of the bending moments with the vertical bars indicating magnitude and the curved arrows indicating direction. Sizable moments occur at the top and bottom ends, $M = 0.19pb^3$ at $y = -b$ and $M = 0.21pb^3$ at $y = +b$. The parts of the rim adjacent to these two ends tend to bend so as to form a smaller radius of curvature than in the unstressed shape. The part around $y = 0$ tends to straighten out, or form a larger radius

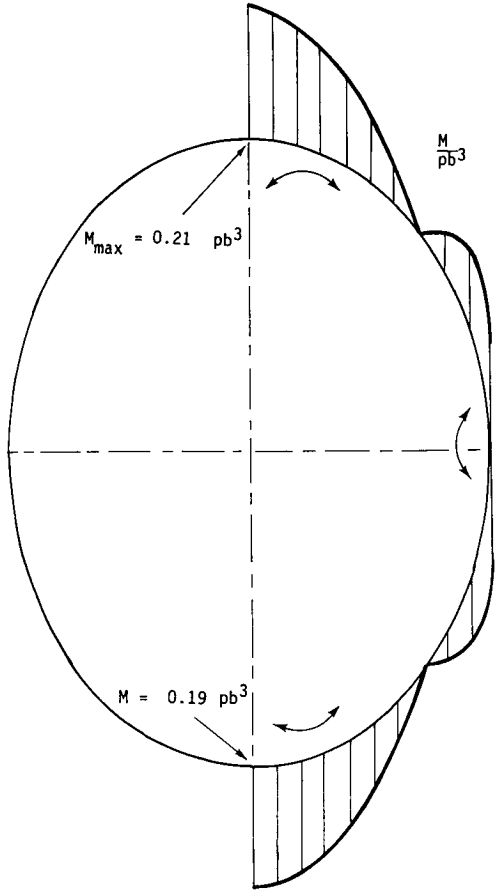

FIG. 8. Distribution along Rim of Internal Moments

of curvature, than in the unstressed shape.

Depending on the relative magnitudes of the area and moment of inertia of the cross section, the bending moments tend to create considerably larger stresses than the shear or compression, and are therefore the predominant factors in determining the strength of the rim support. The critical point is at $y = +b$, which experiences both the largest moment and largest compressive force (Figs. 7 and 8).

Conclusion

A load analysis has been performed for the rim support of an off-axis paraboloidal membrane, such as the deployable solar concentrator. The function of the rim support is to take up the tensile forces created by the stretched membrane. In the analysis, use was made of the off-axis membrane's forming part of a larger, axisymmetrical paraboloid. The meridional and circumferential forces of the latter have been converted to the rim coordinate system

to give the forces transmitted to the rim support. These tensile forces were found to be proportional to pb.

The internal forces and moments generated in the rim support by the membrane forces were calculated. The compression forces are considerably larger, at any point, than the shear forces; both are proportional to pb^2. The bending moments are proportional to pb^3.

The dominant factors in the rim support strength are the bending moments, which generally produce larger stresses than the shear and compression forces. The critical point is at the top of the rim, where both the bending moment and compression force are at their maximum.

Acknowledgment

The writer greatly appreciates the support provided for this project by J. Naujokas, C. Ford, and presently K. Laug of the Air Force Astronautics Laboratory. Thanks are due to G. Pardoen, who reviewed this report and made many useful suggestions. This study was conducted under USAF/AFAL Contract F04611-86-C-0112.

Appendix I. References

Arduini, A., Ponzi, U., and Bernasconi, C. M. (1988). "A contribution to the study of the precise pressurized structures." *Paper No. IAF-88-268, (39th Int. Astronautical Congress)*, International Astronautical Federation, Oct.

Belvin, W. K., Edighoffer, H. H., and Herstrom, C. L. (1987). "Quasi-static shape adjustment of a 15 meter diameter space antenna." AIAA/ASME/ASCE/AHS 28th Struct., *Struct. Dynamics and Matls. Conf.*, American Institute of Aeronautics and Astronautics, Apr., part 1, 705–713.

Grossman, G., and Williams, G. (1989). "Inflatable concentrators for solar propulsion and dynamic space power." *Proc. ASME Int. Solar Energy Conf.*, American Society of Mechanical Engineers, 39–45.

Hedgepeth, J. M. (1985). "New concepts for precision reflector support structure." *Paper No. IAF-85-208, (36th Int. Astronautical Congress)*, International Astronautical Federation, Oct.

Kato, S., et al. (1988). "Concept of inflatable elements supported by truss structure for reflector application." *Paper No. IAF-88-274 (39th Int. Astronautical Congress)*, International Astronautical Federation, Oct.

Marin, J., and Sauer, J. A. (1954). *Strength of materials*. The McMillan Co., New York, N.Y., 238–269.

Popov, E. P. (1952). *Mechanics of materials*. Prentice Hall, Englewood Cliffs, N.J., 525–556.

Roark, R. J. (1971). *Formulas for stress and strain*, McGraw-Hill Book Co., New York, N.Y., 300.

Thomas, M., and Friese, G. J. (1980). "Pressurized antennas for space radars." *Conf. on Sensor Systems for the 80's*, American Institute of Aeronautics and Astronautics, 65–71.

Williams, G. (1987). "Inflatables for lightweight satellite applications." *1st Annual USU Conf. on Small Satellites*, Utah State University, Oct.

Appendix II. Notation

The following symbols are used in this paper:

A = cross-section area (m^2);

B = dimensionless parameter, Eq. 31;
b = one-half of major axis of elliptical rim (m);
C = dimensionless parameter, Eq. 32;
D = dimensionless parameter, Eq. 33;
E = modulus of elasticity (N/m^2);
F = focal length of on-axis, parent paraboloid, Fig. 1 (m);
F_1 = F/b;
F_H = compression/tension force at high cut end of rim, Fig. 5 (N);
F_H^* = F_H/pb^2;
F_L = compression/tension force at low cut end of rim, Fig. 5 (N);
F_L^* = F_L/pb^2;
F_s = shear force in rim (N);
F_s^* = F_s/pb^2;
F_T = compression/tension force in rim (N);
F_T^* = F_T/pb^2;
F_x = internal force in x-direction, Fig. 5 (N);
F_x^* = F_x/pb^2;
F_y = internal force in y-direction, Fig. 5 (N);
F_y^* = F_y/pb^2;
G = shear modulus (N/m^2);
H_1 = dimensionless parameter, Eq. 61;
H_2 = dimensionless parameter, Eq. 62;
I = moment of inertia of cross section (m^4);
i = I/Ab^2;
j = sEI/GAb^2;
K = dimensionless parameter, Eq. 34;
l = arc length along rim, Fig. 2 (m);
M = internal moment, Fig. 5 (N-m);
M^* = M/pb^3;
M_H = internal moment at high cut end of rim, Fig. 5 (N-m);
M_H^* = M_H/pb^3;
M_L = internal moment at low cut end of rim, Fig. 5 (N-m);
M_L^* = M_L/pb^3;
p = inflation pressure (N/m^2);
R_c = radius of curvature in circumferential direction (m);
R_m = radius of curvature in meridional direction (m);
r = radial coordinate of on-axis, parent paraboloid, Fig. 1 (m);
r_A = radial coordinate of point A, where meridian is tangent to rim, Fig. 1 (m);
S_c = arc length in circumferential direction, Fig. 2 (m);
S_m = arc length in meridional direction, Fig. 2 (m);
s = factor in Eq. 52 expressing nonuniform distribution of shear stresses over cross section;
T = tensile force in circumferential direction (N/m);
T_c = circumferential tensile force (N/m);
T_m = meridional tensile force (N/m);
T_n = tensile force exerted by membrane normal to rim plane (N/m);
T_n^* = T_n/pb;
T_r = tensile force in radial direction (N/m);
T_s = tensile force in direction normal to rim (N/m);
T_T = tensile force in direction tangential to rim (N/m);

T_x = tensile force exerted by membrane or rim support in x-direction (N/m);
T_x^* = T_x/pb;
T_y = tensile force exerted by membrane on rim support in y-direction (N/m);
T_y^* = T_y/pb;
T_z = tensile force in axial direction (N/m);
U = strain energy, Eq. 52 (J);
x = rim coordinate along minor axis (m);
y = rim coordinate along major axis (m);
y_1 = y/b;
z = axial coordinate of on-axis, parent paraboloid, Fig. 1 (m);
β = angle of inclination of off-axis rim, Fig. 1 (rad);
γ = slope angle of elliptical rim, Fig. 2 (rad);
δ = slope angle of on-axis, parent paraboloid, Fig. 1 (rad); and
θ = circumferential coordinate of on-axis, parent paraboloid, Fig. 1 (rad).

Analysis of Rim Supports for Off-Axis Inflatable Reflectors. II: Deformations

By Gershon Grossman[1]

Abstract: A structural analysis is performed for the rim support of a pressurized off-axis paraboloidal membrane, serving as a space-based solar concentrator. The function of the rim support is to take up the tensile forces created by the stretched membrane. This paper analyzes the deformations in the rim support, based on an earlier evaluation of the internal forces and moments resulting from the load applied by the membrane. The deformations are calculated in the x- and y-directions at all points along the rim. They are shown to depend on the rim geometry, the applied loads, and a dimensionless rigidity parameter comprising the inflation pressure, the major axis of the elliptical rim, the modulus of elasticity of the rim support material, and its moment of inertia. The angular deformation at each point is also evaluated. A simplified solution for small deformations shows them to be approximately proportional to the rigidity parameter.

Introduction

The purpose of the present analysis has been to calculate the deformations in the rim support of the deployable solar concentrator, a lightweight inflatable device providing solar heat at high temperature to a hydrogen engine aboard a solar rocket. The latter is a vehicle designed to carry payloads from a low earth orbit (LEO) to a geosynchronous orbit (GEO) at significant mass savings compared to the more conventional chemical propulsion. The deployable solar concentrator, its geometry, and its structure have been described in detail by Grossman and Williams (1989). It consists of a plane rim support in the form of an elliptical torus that carries two geometrically identical membranes, one serving as a reflector and the other as a canopy, in an off-axis paraboloidal configuration.

A companion paper (Grossman 1991) has described an analysis of the loads exerted on the rim support by the membranes. The deformations depend directly on the loads, as well as on the geometry and elastic properties of the rim support material. In the present paper, frequent reference is made to the load analysis, and the same notation is employed, where applicable. The reader is urged to familiarize himself with the load analysis in the companion paper before proceeding.

Deformation Analysis

Fig. 1(a) describes schematically the elliptical rim in the same x-y coordinate system employed in the load analysis (Grossman 1991). The solid

[1]Prof., Dept. of Mech. Engrg., Technion, Israel Inst. of Tech., 32000 Haifa, Israel; formerly Program Engr., L'Garde, Inc., 15181 Woodlawn Ave., Tustin, CA 02680.

Note. Discussion open until June 1, 1991. Separate discussions should be submitted for the individual papers in this symposium. To extend the closing date one month, a written request must be filed with the ASCE Manager of Journals. The manuscript for this paper was submitted for review and possible publication on April 27, 1989. This paper is part of the ***Journal of Aerospace Engineering***, Vol. 4, No. 1, January, 1991. ©ASCE, ISSN 0893-1321/91/0001-0067/$1.00 + $.15 per page. Paper No. 25374.

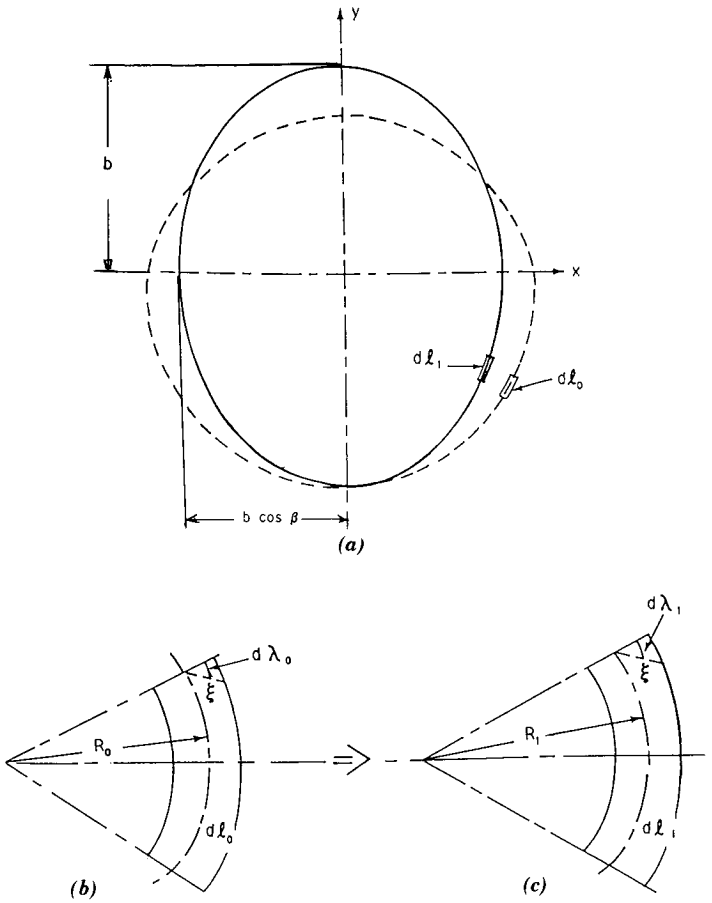

FIG. 1. Geometry of Deforming Rim Support: (*a*) Unstressed Rim (Broken Line, Index 0) and Stressed Rim (Solid Line, Index 1); (*b*) Element of Unstressed Rim; and (*c*) Element of Stressed Rim

and broken lines represent the stressed and unstressed shape, respectively. It is required that the rim assume the design elliptical contour when subject to the load; therefore, the solid line describes a perfect ellipse, whereas the shape of the broken line is to be calculated. A small element dl_0 of the unstressed rim becomes d_{l1} when the rim is stressed, as shown.

Figs. 1(*b*) and 1(*c*) describe the rim-support elements dl_0 and dl_1 in a magnified form. The elements dl_0 and dl_1 actually represent the lengths of the arc along the neutral line. In addition to this length change, the radius of curvature of the rim-support element along the neutral line varies, when stressed, from R_0 to R_1. As the element bends, the angle between the planes defining its two end cross sections changes as well. Let us consider a "fiber" of the rim support material located a distance ξ from the neutral line. Under stress, it changes its length from $(dl_0 + d\lambda_0)$ to $(dl_1 + d\lambda_1)$, where $d\lambda$ is the

amount by which the fiber is longer than the neutral line. The strain in this fiber is given by

$$\epsilon = \frac{(dl_1 + d\lambda_1) - (dl_0 + d\lambda_0)}{dl_0 + d\lambda_0} \quad \ldots\ldots (1)$$

Is is easy to show by similarity of triangles in Figs. 1(*b*) and 1(*c*) that

$$d\lambda_0 = \xi \frac{dl_0}{R_0} \quad \ldots\ldots (2a)$$

$$d\lambda_1 = \xi \frac{dl_1}{R_1} \quad \ldots\ldots (2b)$$

From the results of the load analysis, considering the effects of both bending and compression, the stress in the fiber is

$$\sigma = \frac{F_T}{A} + \frac{M}{I}\xi \quad \ldots\ldots (3)$$

where F_T = the tension force (or compression, when negative); M = the bending moment exerted on the element by the external load; and A and I = the area and moment of inertia, respectively, of the rim-support cross section. Denoting the elastic modulus of the material by E and using the elastic stress-strain relation we obtain from Eqs. 1 and 3

$$\frac{dl_1 + d\lambda_1}{dl_0 + d\lambda_0} - 1 = \frac{1}{E}\left(\frac{F_T}{A} + \frac{M}{I}\xi\right) \quad \ldots\ldots (4)$$

and substituting the values of $d\lambda_0$ and $d\lambda_1$ from Eq. 2

$$dl_1\left(1 + \frac{\xi}{R_1}\right) = \left[1 + \frac{1}{E}\left(\frac{F_T}{A} + \frac{M}{T}\xi\right)\right] dl_0\left(1 + \frac{\xi}{R_0}\right) \quad \ldots\ldots (5)$$

In particular, for the neutral line ($\xi = 0$)

$$dl_1 = dl_0\left(1 + \frac{F_T}{EA}\right) \quad \ldots\ldots (6)$$

subtracting Eq. 6 from Eq. 5 and rearranging, we find

$$\left(1 + \frac{F_T}{EA}\right)\left(\frac{1}{R_1} - \frac{1}{R_0}\right) = \frac{M}{EI}\left(1 + \frac{\xi}{R_0}\right) \quad \ldots\ldots (7)$$

and since $\xi << R_0$ everywhere, ϵ/R_0 may be neglected.

The radius of curvature and arc length of the rim may be expressed in terms of the x-y coordinates as follows (Popov 1976):

$$dl = (dx^2 + dy^2)^{1/2} \quad \ldots\ldots (8)$$

$$\frac{1}{R} = \frac{\dfrac{d^2y}{dx^2}}{\left[1 + \left(\dfrac{dy}{dx}\right)^2\right]^{3/2}} \quad \ldots\ldots (9)$$

substituting in Eqs. 6 and 7 we obtain

$$\left(\frac{dx_1^2 + dy_1^2}{dx_0^2 + dy_0^2}\right)^{1/2} = 1 + \frac{F_T}{EA} \quad \text{(10)}$$

$$\frac{\dfrac{d^2y_1}{dx_1^2}}{\left[1 + \left(\dfrac{dy_1}{dx_1}\right)^2\right]^{3/2}} - \frac{\dfrac{d^2y_0}{dx_0^2}}{\left[1 + \left(\dfrac{dy_0}{dx_0}\right)^2\right]^{3/2}} = \frac{\dfrac{M}{EI}}{\left(1 + \dfrac{F_T}{EA}\right)} \quad \text{(11)}$$

Eq. 10 may be rewritten as

$$\left[1 + \left(\frac{dy_0}{dx_0}\right)^2\right]\left(1 + \frac{F_T}{EA}\right)^2\left(\frac{dx_0}{dx_1}\right)^2 = 1 + \left(\frac{dy_1}{dx_1}\right)^2 \quad \text{(12)}$$

and finally, combining Eqs. 12 and 11 yields

$$\frac{d^2y_0}{dx_0^2}\left(1 + \frac{F_T}{EA}\right)^3\left(\frac{dx_0}{dx_1}\right)^3 = \frac{d^2y_1}{dx_1^2} - \frac{\dfrac{M}{EI}}{\left(1 + \dfrac{F_T}{EA}\right)}\left[1 + \left(\frac{dy_1}{dx_1}\right)^2\right]^{3/2} \quad \text{(13)}$$

Eqs. 12 and 13 may be solved together for x_0 and y_0, in terms of y_1. Note that x_1 is known in terms of y_1 from the equation of the ellipse:

$$\frac{x_1^2}{\cos^2\beta} + y_1^2 = b^2 \quad \text{(14)}$$

Also, F_T and M are known in terms of y_1 from the load analysis (Grossman 1991). Thus, the simultaneous solution of Eqs. 12 and 13 would yield the unstressed shape of the rim.

It is interesting to note that in the case of no compression, $F_T = 0$, Eq. 12 yields $dx_0^2 + dy_0^2 = dx_1^2 + dy_1^2$, which means no change in length of the element's neutral line when stressed. Also, substituting $dy_0/dx_0 = d^2y_0/dx_0^2 = 0$ in Eq. 13 in addition to $F_T = 0$ yields the familiar formula for pure bending of a straight beam (Popov 1976).

Solution

To solve Eqs. 12 and 13, let us define

$$\tan\psi = \frac{dy_0}{dx_0} \quad \text{(15a)}$$

$$c = 1 + \frac{F_T}{EA} = 1 + \left(\frac{pb^2}{EA}\right)F_T^* \quad \text{(15b)}$$

where ψ = the slope angle of the unstressed rim; and c = a dimensionless compression parameter. Substituting in Eqs. 12 and 13 yields

$$c^2(1 + \tan^2\psi)\left(\frac{dx_0}{dx_1}\right)^2 = 1 + \left(\frac{dy_1}{dx_1}\right)^2 \quad \text{(16)}$$

$$c^3\frac{d(\tan\psi)}{dx_0}\left(\frac{dx_0}{dx_1}\right)^3 = \frac{d^2y_1}{dx_1^2} - \frac{\dfrac{M}{EI}}{c}\left[1 + \left(\frac{dy_1}{dx_1}\right)^2\right]^{3/2} \quad \text{(17)}$$

Assuming $dx_0/dx_1 \neq 0$ everywhere (to be confirmed later), Eq. 17 may be divided by Eq. 16 to give

$$\frac{\dfrac{d(\tan\psi)}{dx_1}}{1 + \tan^2\psi} = \frac{1}{c}\left[\frac{\dfrac{d^2y_1}{dx_1^2}}{1 + \left(\dfrac{dy_1}{dx_1}\right)^2} - \sqrt{1 + \left(\frac{dy_1}{dx_1}\right)^2}\,\frac{M}{cEI}\right] \quad \text{(18)}$$

The right-hand side of Eq. 18 is known as a function of y_1; x_1 is given in terms of y_1 by the elliptical geometry, Eq. 14; M and c are known from the load analysis (Grossman 1991). Eq. 18 may therefore be rewritten as follows:

$$d\psi = \left[\frac{\dfrac{d^2y_1}{dx_1^2}}{1 + \left(\dfrac{dy_1}{dx_1^2}\right)} - \sqrt{1 + \left(\frac{dy_1}{dx_1}\right)^2}\,\frac{\dfrac{M}{EI}}{c}\right]\left(\frac{dx_1}{\dfrac{dy_1}{c}}\right)dy_1 \quad \text{(19)}$$

When one is performing the integration, a boundary condition is required. From symmetry considerations [Fig. 1(*a*)] we note that at $y = -b$, $dy_0/dx_0 = 0$ and therefore also $\psi = 0$. Eq. 19 thus yields

$$\psi = \int_{-b}^{y_1} \frac{\dfrac{d}{dy_2}\left(\dfrac{dy_2}{dx_2}\right)}{1 + \left(\dfrac{dy_2}{dx_2}\right)^2} - \sqrt{1 + \left(\frac{dx_2}{dy_2}\right)^2}\,\frac{\dfrac{M}{EI}}{c}\frac{dy_2}{c} \quad \text{(20)}$$

where y_2 and x_2 = variables of integration. Note that in the no-load case, substituting $M = 0$ and $c = 1$ in Eq. 20, we find $\psi = \arctan(dy_1/dx_1)$, which indicates no deformation, as should be the case.

From Eq. 16 we now obtain

$$\frac{dx_0}{dx_1} = \frac{1}{c}\left[\frac{1 + \left(\dfrac{dy_1}{dx_1}\right)^2}{1 + \tan^2\psi}\right]^{1/2} \quad \text{(21)}$$

and using the definition of the slope angle

$$\frac{dy_0}{dx_1} = \frac{dy_0}{dx_0}\frac{dx_0}{dx_1} = \tan\psi\,\frac{dx_0}{dx_1} \quad \text{(22)}$$

Rearranging the terms, we finally obtain

$$\frac{dx_0}{dy_1} = \sqrt{1 + \left(\frac{dx_1}{dy_1}\right)^2}\,\frac{\cos\psi}{c} \quad \text{(23a)}$$

$$\frac{dy_0}{dy_1} = \sqrt{1 + \left(\frac{dx_1}{dy_1}\right)^2}\,\frac{\sin\psi}{c} \quad \ldots\ldots (23b)$$

which may be integrated with respect to y_1 to find x_0 and y_0 at all points and hence the shape of the unstressed rim. Substituting the relation between y_1 and x_1 from the shape of the ellipse, Eq. 14, and arranging the terms in dimensionless groups, we find

$$\frac{dx_0}{dy_1} = \left[\frac{1 - \left(\frac{y_1}{b}\right)^2 \sin^2\beta}{1 - \left(\frac{y_1}{b}\right)^2}\right]^{1/2} \frac{\cos\psi}{c} \quad \ldots\ldots (24a)$$

$$\frac{dy_0}{dy_1} = \left[\frac{1 - \left(\frac{y_1}{b}\right)^2 \sin^2\beta}{1 - \left(\frac{y_1}{b}\right)^2}\right]^{1/2} \frac{\sin\psi}{c} \quad \ldots\ldots (24b)$$

$$\psi = \int_{-1}^{y_1/b} \left[\frac{\cos\beta}{(1 - y_2^2 \sin^2\beta)^{3/2}} - \left(\frac{pb^4}{EI}\right)\frac{M^*}{c}\right] \sqrt{\frac{1 - y_2^2 \sin^2\beta}{1 - y_2^2}}\,\frac{dy_2}{c} \quad \ldots\ldots (25)$$

where $M^* = (M/pb^3)$ is the dimensionless bending moment (Grossman 1991).

Having found the shape of the unstressed rim support, it is now possible to calculate the deformations. At each point, the deformation may be defined in terms of its x- and y-components, u and v, respectively

$$u = (x_1 - x_0) \qquad v = (y_1 - y_0) \quad \ldots\ldots (26)$$

Since the deformations are small in comparison to the initial rim dimensions, calculating x_0, y_0 from Eq. 24 and then subtracting from x_1, y_1 will cause a numerical error resulting from the need to take a small difference between two large numbers. Rather than doing this, we will attempt to derive an expression for u and v. From Eqs. 26, 23, and 8

$$du = \left(\frac{dx_1}{\sqrt{dx_1^2 + dy_1^2}} - \frac{\cos\psi}{c}\right) dl_1 \quad \ldots\ldots (27a)$$

$$dv = \left(\frac{dy_1}{\sqrt{dx_1^2 + dy_1^2}} - \frac{\sin\psi}{c}\right) dl_1 \quad \ldots\ldots (27b)$$

The slope of the stressed rim, ϕ, is defined by

$$\phi = \arctan\left(\frac{dy_1}{dx_1}\right) \quad \ldots\ldots (28)$$

substituting ϕ from Eq. 28 and c from Eq. 15b in Eq. 27 yields

$$du = \left[\cos\phi - \cos\psi + \left(\frac{pb^2}{EA}\right) F_T^* \cos\phi\right] \frac{dl_1}{c} \quad \ldots\ldots (29a)$$

$$dv = \left[\sin\phi - \sin\psi + \left(\frac{pb^2}{EA}\right) F_T^* \sin\phi\right] \frac{dl_1}{c} \quad \ldots\ldots (29b)$$

which may be rewritten as

$$du = \left[2 \sin\left(\frac{\psi + \phi}{2}\right) \sin\left(\frac{\psi - \phi}{2}\right) + \left(\frac{pb^2}{EA}\right) F_T^* \cos\phi\right] \frac{dl_1}{c} \quad \ldots\ldots (30a)$$

$$dv = \left[-2 \cos\left(\frac{\psi + \phi}{2}\right) \sin\left(\frac{\psi - \phi}{2}\right) + \left(\frac{pb^2}{EA}\right) F_T^* \sin\phi\right] \frac{dl_1}{c} \quad \ldots\ldots (30b)$$

Note that the term $\sin(\psi - \phi)/2$ in both Eqs. 30a and 30b can be quite small if the deformation is small and the slope angles of the stressed and unstressed rim are close to each other; (pb^2/EA) in the next term can be quite small too, particularly for stiff materials. Thus, du and dv are each expressed as the sum of two small numbers, rather than as the difference of two large numbers. The numerical error in the former is much smaller than in the latter, making the former convenient for computer calculations.

Finally, from the definitions of ψ and ϕ, Eqs. 20 and 28, we find

$$\psi \pm \phi = \int_{-b}^{y_1} \left[\frac{\frac{d^2y_2}{dx_2^2}}{\left[1 + \left(\frac{dy_2}{dx_2}\right)^2\right]^{3/2}} (1 \pm c) - \frac{\frac{M}{EI}}{c}\right] \frac{dl_2}{c} \quad \ldots\ldots (31a)$$

and substituting the relation between x_1 and y_1 from the shape of the ellipse, Eq. 14

$$\psi \pm \phi = \int_{-1}^{(y_1/b)} \left[\frac{\cos\beta}{(1 - y_2^2 \sin^2\beta)^{3/2}} (1 \pm c) - \left(\frac{pb^4}{EI}\right)\frac{M^*}{c}\right] \sqrt{\frac{1 - y_2^2 \sin^2\beta}{1 - y_2^2}}\,\frac{dy_2}{c} \quad \ldots (31b)$$

The value of $(\psi \pm \phi)$, obtained by a simple numerical integration from Eq. 31b, is substituted in Eqs. 30a and b, which are integrated to give the deformations u and v at all points along the rim.

RESULTS

The results of the foregoing analysis have been expressed in dimensionless form, for clarity and generality. The analysis has yielded the dimensionless deformations in the x- and y-directions, u/b and v/b, respectively, at all points along the rim, as functions of the following parameters: (1) The rim geometry, as expressed by cos, the ratio of the minor to major axis of the ellipse; (2) the applied membrane load, as expressed by M^*, the dimensionless moment, and c, involving the dimensionless compression force, F_T^*, and (3) the rigidity parameters I/Ab^2 and pb^4/EI, involving the elastic properties of the rim support material and its cross-section area and moment of inertia.

Fig. 2 describes the stressed and unstressed shape of the rim support for the particular geometry of the deployable solar concentrator (Grossman and Williams 1989): $F = 3.186$ m, $b = 4.57$ m, $\beta = 40°$. M^* and F_T^* for this geometry are uniquely determined from the load analysis (Grossman 1991) (note that $i = I/Ab^2$ is very small). A typical value of $pb^4/EI = 1.384$ has been selected. This value is based on the inflation pressure and dimensions

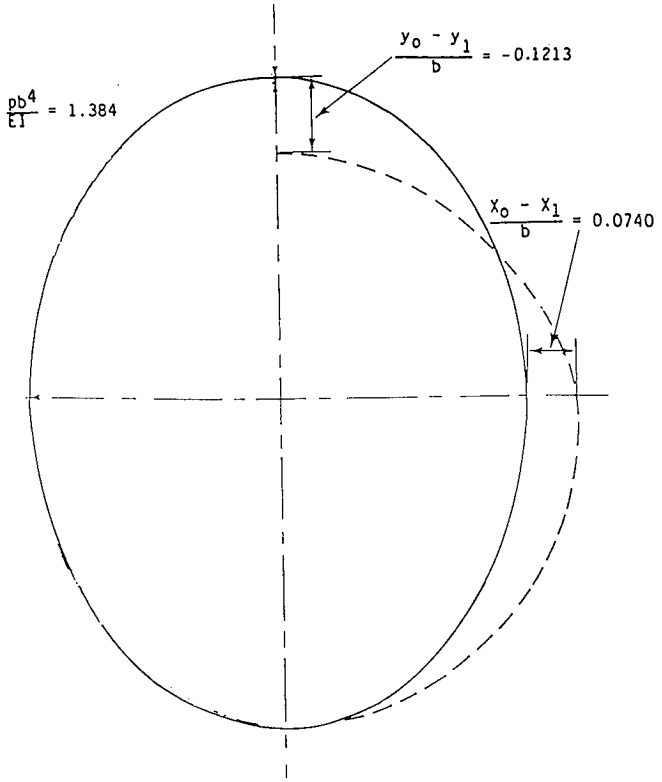

FIG. 2. Stressed and Unstressed Shape of Rim Support for DSCE Geometry, for Typical Value of Rigidity Parameter (pb^4/EI) = 1.384

calculated for the 9 × 7-m reflector, and on the properties of polyurethane foam—one candidate material for a rigidized rim support. The integration of Eqs. 30 and 31 leading to these results has been performed numerically.

Fig. 2 shows the maximum x- and y-deviations between the stressed and unstressed rim. It is clear that with the present foam, the deviation is quite significant. A more rigid rim support with a higher value of pb^4/EI would give smaller deviations. It is evident that the unstressed shape is closer to circular than the stressed. The applied moments tend to reduce the radius of curvature at the major axis and increase it at the minor axis. This had already been observed when the moment distribution was calculated (Grossman 1991).

Fig. 3 describes the variation of the maximum deformations in the x- and y-directions, u at the minor axis, and v at the major axis, respectively, with the rigidity parameter pb^4/EI. The results were calculated for the deployable solar concentrator (DSCE) geometry and for $i = 0$. It is evident that both deformations increase with pb^4/EI. A simplified formula may be derived for the case where pb^4/EIE is very small, leading to very small deformations. Substituting $(\psi - \phi) \approx 2\phi$, $\sin(\psi - \phi) \approx \psi - \phi$, $c \approx 1$ in Eqs. 30a and b yields

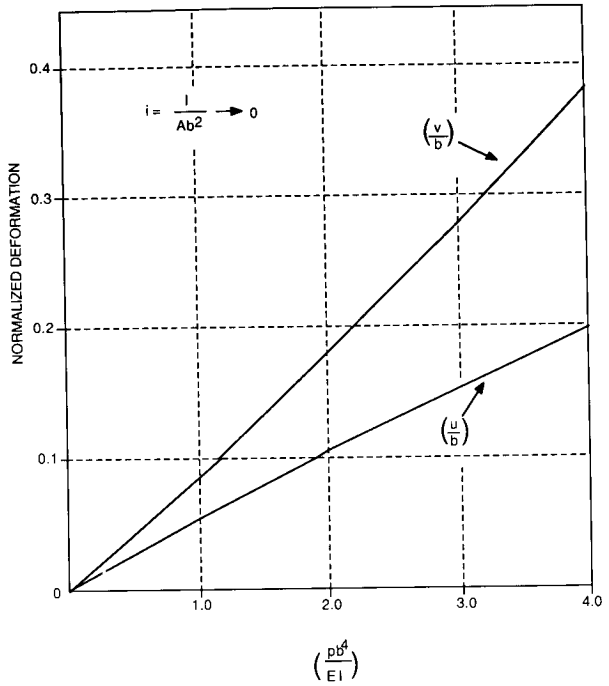

FIG. 3. Normalized Maximum Deformations in x- and y-Directions (u/b and v/b, Respectively) as Functions of Rigidity Parameter (pb^4/EI), for Deployable Solar Concentrator Geometry and $i = 0$

$$du = \left[(\psi - \phi)\sin\phi + i\left(\frac{pb^4}{EI}\right)F_T^*\cos\phi\right]dl_1 \quad (32a)$$

$$dv = \left[-(\psi - \phi)\cos\phi + i\left(\frac{pb^4}{EI}\right)F_T^*\sin\phi\right]dl_1 \quad (32b)$$

The term $\psi - \phi$ may in turn be obtained from Eq. 31b

$$\psi - \phi = -\frac{pb^4}{EI}\int_{-1}^{y_1/b}\left[\frac{\cos\beta}{(1 - y_2^2\sin^2\beta)^{3/2}}iF_T^* + M^*\right]dl_2 \quad (33)$$

Note that the integral in Eq. 33 is independent of the rigidity and depends only on the geometry of the rim support. Thus, both du and dv in Eqs. 32a and b are proportional to pb^4/EI. In particular, for the case of $i << 1$ the bending moments dominate:

$$du = \frac{pb^4}{EI}\left(-\sin\phi\int_{-1}^{y_1/b}M^*dl_2\right)dl_1 \quad (34a)$$

$$dv = \frac{pb^4}{EI}\left(\cos\phi\int_{-1}^{y_1/b}M^*dl_2\right)dl_1 \quad (34b)$$

Conclusion

A deformation analysis has been performed for the rim support of an off-axis paraboloidal membrane, such as the deployable solar concentrator. The function of the rim support is to take up the tensile forces created by the stretched membrane. The deformations result from the loads applied by the membrane on the rim support (predominantly bending and compression) that have been calculated in a companion paper (Grossman 1991).

The analysis gives the deformations in the x- and y-directions (u and v, respectively) at all points along the rim. The deformations are shown to depend on the rim geometry, the applied loads, and a rigidity parameter pb^4/EI. When deformations are small, they are approximately proportional to pb^5/EI.

Acknowledgments

The writer greatly appreciates the support provided for this project by J. Naujokas, C. Ford, and presently K. Laug of the Air Force Astronautics Laboratory. This study was conducted under USAF/AFAL contract F04611-86-C-0112.

Appendix I. References

Grossman, G. (1991). "Analysis of rim supports of off-axis inflatable reflectors. I: Loads." *J. Aerospace Engrg.*, ASCE, 4(1), 47–66 .

Grossman, G., and Williams, G. (1989). "Inflatable concentrators for solar propulsion and dynamic space power." *Proc. ASME Int. Solar Energy Conf.*, American Society of Mechanical Engineers, 39–45.

Popov, E. P. (1976). *Mechanics of materials*. Prentice Hall, Englewood Cliffs, N.J., 355–357.

Appendix II. Notation

The following symbols are used in this paper:

A = cross-section area (m^2);
b = half of major axis of elliptical rim (m);
c = dimensionless compression parameter, Eq. 15*b*;
E = modulus of elasticity (N/m^2);
F = focal length of on-axis, parent paraboloid (m);
F_1 = F/b (dimensionless);
F_T = compression/tension force in rim, (N);
F_T^* = F_T/pb^2;
I = moment of inertia of cross section (m^4);
i = I/Ab^2;
l = arc length along rim, Fig. 1 (m);
M = integral moment, (N-m);
M^* = M/pb^3;
p = inflation pressure (N/m^2);
R = radius of curvature of rim (m);
u = deformation in x-direction, Eq. 26 (m);
v = deformation in y-direction, Eq. 26 (m);
x = rim coordinate along minor axis (m);
y = rim coordinate along major axis (m);
β = angle of inclination of off-axis rim, (rad);
ϵ = strain;
λ = length increment over neutral line, Fig. 1 (m);
ξ = distance from neutral line, Fig. 1 (m);
σ = stress;
ϕ = slope angle of stressed rim (radians); and
ψ = slope angle of unstressed rim (radians).

Subscripts

0 = unstressed rim;
1 = stressed rim; and
2 = variable of integration.

TENSION ELEMENT TO REDUCE LOADS IN RIM SUPPORT OF INFLATABLE REFLECTOR

By Gershon Grossman[1]

ABSTRACT: A structural analysis is performed for the rim support of a pressurized off-axis paraboloidal membrane that serves as a space-based solar concentrator. The function of the elliptical rim support is to take up the tensile forces created by the stretched membrane. This paper extends earlier load and deformation analyses to include the effect of a tension element added along the major axis of the ellipse. Such an element, in the form of a string or cable, restrains the tendency for increased ovality of the rim support under load without seriously interfering with the packaging and deployment of the device, at negligible added mass. The internal forces and moments and the deformations resulting from the membrane-applied loads have been calculated. The analysis has shown that a properly designed tension element can reduce the maximum bending moment by more than a factor of 2. The deformations are reduced by more than a factor of 20.

INTRODUCTION

Inflatable structures employing thin, pressurized membranes for use in space have received growing attention in the past few years in view of their many potential applications. Among those, perhaps the most important ones are solar concentrators and space antennas. In both applications, the membrane must assume a geometrical shape of considerable accuracy. The designer is faced with the task of supporting the membrane at the rim against sizable forces. The rim support must have not only the strength to carry the load imposed by the inflation pressure, but also the rigidity to resist deformation and allow the membrane to maintain its accurate shape.

Two earlier studies (Grossman 1991) have considered the loads and deformations created in the rim support of an off-axis inflatable paraboloidal membrane, such as the one for the Deployable Solar Concentrator (Grossman and Williams 1989, 1990; Williams 1987). The forces transmitted by the stretched membrane to the rim support create in the latter internal shear and compression forces as well as sizable bending moments, due to the nonsymmetrical pattern and compression forces as well as sizable bending moments, due to the nonsymmetrical pattern of the membrane forces. These loads result in a deformation of the rim support, which may be deleterious to the accuracy of the paraboloid if not taken into consideration properly. The load analysis (Grossman, 1991) showed the membrane forces to be on the order of (pb), the internal forces on the order of (pb^2), and the moments on the order of (pb^3), where p is the inflation pressure; and b is half the major axis of the elliptical rim. The deformation analysis (Grossman 1991) showed that when deformations are small, they are on the order of (pb^5/EI), where E is the modulus of elasticity of the rim support material, and I is the moment of inertia of its cross section. The pattern of deformation

[1]Prof., Fac. of Mech. Engrg., Technion—Israel Inst. of Technol., Haifa 3200, Israel.

Note. Discussion open until September 1, 1994. To extend the closing date one month, a written request must be filed with the ASCE Manager of Journals. The manuscript for this paper was submitted for review and possible publication on April 7, 1992. This paper is part of the ***Journal of Aerospace Engineering***, Vol. 7, No. 2, April, 1994. ©ASCE, ISSN 0893-1321/94/0002-0129/$2.00 + $.25 per page. Paper No. 3824.

is toward an increase in the ovality of the ellipse; that is, the major axis tends to elongate and the minor axis tends to become shorter.

The purpose of the present study has been to investigate the possibility of reducing both loads and deformation by adding a tension-resisting element such as high-modulus cable along the major axis of the ellipse. As is shown, such an element would act against the deformation tendency of the rim support. A compression-resisting spoke along the minor axis would have a similar effect, but is not desirable for practical reasons: it would be considerably heavier, having to resist buckling, and harder to package.

INTERNAL FORCES AND MOMENTS

The first step in the earlier load analysis (Grossman 1991) was to calculate the membrane forces transmitted to the rim support. The same forces T_x and T_y in the x- and y-directions, respectively, are in effect under the present conditions. Their distribution along the elliptical rim, as calculated in the earlier load analysis (Grossman 1991), is illustrated in Fig. 1 for the geometry of the Deployable Solar Concentrator (Grossman and Williams 1989, 1990):

$$F = 3.186 \text{ m}; \quad b = 4.57 \text{ m}; \quad \beta = 40^\circ \qquad (1a,b,c)$$

The rim loading is clearly symmetrical with respect to the y-axis; T_x is

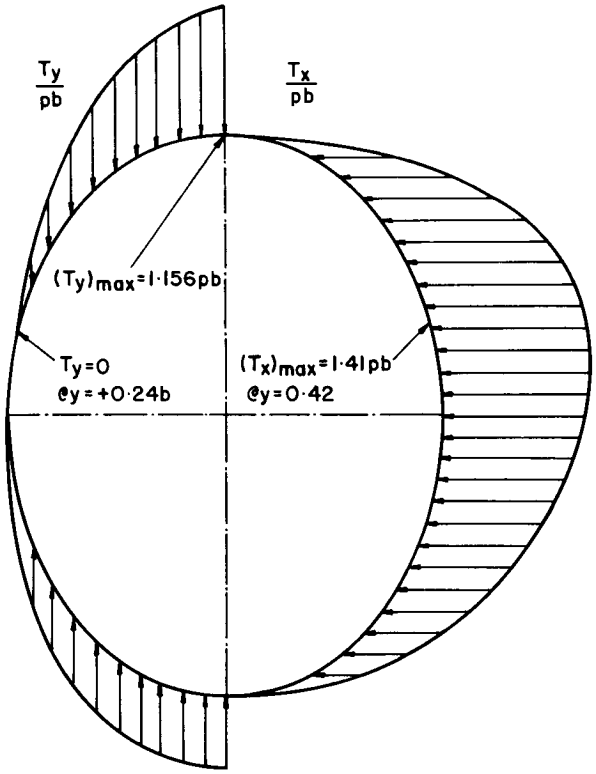

FIG. 1. Distribution along Rim of Membrane-Applied Tensile Forces in x- and y-Directions (Grossman 1991)

shown in the right part of Fig. 1 and T_y in the left; however, it is clear that each point on the rim has both T_x and T_y acting on it in their respective directions.

Fig. 2(a) shows the elliptical rim support with the tension element along the major axis, applying a tension force $P = k\delta$ when the membrane is inflated; δ is the elastic elongation of the cable with respect to its unloaded length, and k is its spring constant. To calculate the internal forces and moments we employ a free-body method, in which the rim support is cut and a portion of it, subject to internal loading, is studied. As in the earlier load analysis (Grossman 1991), we take advantage of the symmetry with respect to the y-axis and make the first cut along this axis, as illustrated in Fig. 2(b). The reactions at the two cut ends are marked by F_L, M_L at the low end and F_H, M_H at the high end. Symmetry allows only internal forces normal to the cross section, that is in the x-direction, and bending moments, as shown. Also shown are the forces $P/2$ applied by the tension element at each end. Force balances on the right half of the rim support in the x- and y-directions yield

$$\sum P_x = F_L + F_H + \int_{y=-b}^{+b} T_x \, dl = 0 \qquad (2)$$

$$\sum P_y = \int_{y=-b}^{+b} T_y \, dl + \frac{P}{2} - \frac{P}{2} = 0 \qquad (3)$$

A moment balance about the low-cut end gives

$$\sum M = M_L + M_H - 2bF_H + \int_{y=-b}^{+b} xT_y \, dl - \int_{y=-b}^{+b} (y + b)T_x \, dl = 0 \qquad (4)$$

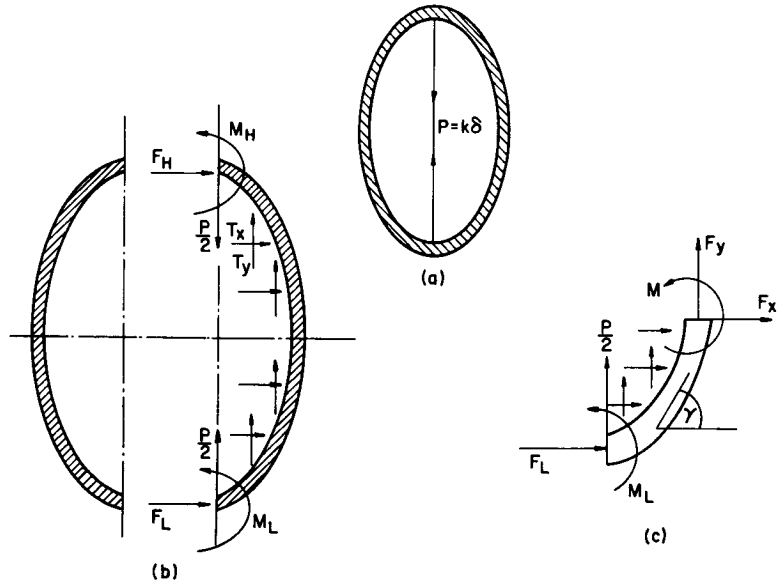

FIG. 2. Internal Forces and Moments in Rim Support: (a) Force Applied by Tension Element; (b) Cut along Axis of Symmetry; (c) Loads Applied to Rim Element

Eq. (3) does not provide any new information, since the terms with $P/2$ cancel out. It merely provides a check on T_y, which was calculated in the earlier load analysis (Grossman 1991), to confirm that y tensile forces on the rim are balanced. We thus have two equations, (2) and (4), for the five unknowns (F_L, F_H, M_L, M_H, and P). The problem is clearly statically indeterminate.

Additional information on this type of problem must be obtained from an analysis of the deformations. In this particular example, due to the symmetry with respect to the y-axis, it is required that the horizontal deflections as well as the angular deformations at the cut ends be zero; the vertical deflections of the cut ends are $\delta = P/k$, inward. We employ Castigliano's second theorem (Marin and Sauer 1954) which makes use of the strain energy U, calculated in terms of the unknown reactions. To obtain the three additional equations required to solve the present problem, we express U in terms of M_L, F_L, and P, and require that

$$\partial U/\partial M_L = 0 \tag{5}$$

$$\partial U/\partial F_L = 0 \tag{6}$$

$$\partial U/\partial P = -P/k \tag{7}$$

The total strain energy contains terms associated with tension/compression, shear and bending of the rim support. To calculate it, we must find the normal and tangential forces and the bending moments at each cross section. To this end, we cut the right half of the rim support further, at an arbitrary point, as shown in Fig. 2(c). Internal forces F_x, F_y and a bending moment M, act at the cut end, as shown. A force balance in the x- and y-directions and a sum of moments about the low-cut end give three equations, for F_x, F_y, and M, in terms of the three still unknown reactions F_L, M_L, and P

$$\sum P_x = F_L + F_x + \int_{y=-b}^{y} T_x\, dl = 0 \tag{8}$$

$$\sum P_y = \frac{P}{2} + F_y + \int_{y=-b}^{y} T_y\, dl = 0 \tag{9}$$

$$\sum M = M_L + M - (y + b)F_x + xF_y - \int_{y=-b}^{y} (y + b)T_x\, dl + \int_{y=-b}^{y} xT_y\, dl = 0 \tag{10}$$

It is convenient to normalize the forces and moments, and introduce the following dimensionless equivalents:

$$\left.\begin{aligned} &T_x^* = T_x/(pb); \qquad T_y^* = T_y/(pb) \\ &P^* = P/(pb^2) \\ &F_x^* = F_x/(pb^2);\ F_y^* = F_y/(pb^2);\ F_L^* = F_L/(pb^2);\ F_H^* = F_H/(pb^2) \\ &M^* = M/(pb^3);\ M_L^* = M_L/(pb^3);\ M_H^* = M_H/(pb^3) \end{aligned}\right\} \tag{11}$$

Substituting the internal forces and moments in (8)–(10) we can solve for the internal forces and moments

$$F_x^*(y) = -F_L^* - \int_{-1}^{y_1} T_x^* K\, dy_2 \tag{12}$$

$$F_y^*(y) = -\frac{P^*}{2} - \int_{-1}^{y_1} T_y^* K\, dy_2 \tag{13}$$

$$M^*(y) = -M_L^* - (1 + y_1)F_L^* - (1 + y_1)\int_{-1}^{y_1} T_x^* K\, dy_2 + \sqrt{1 - y_1^2}\cos\beta \int_{-1}^{y_1} T_y^* K\, dy_2 + \sqrt{1 - y_1^2}\cos\beta\,\frac{P^*}{2} + \int_{-1}^{y_1} (1 + y_2)T_x^* K\, dy_2 - \cos\beta \int_{-1}^{y_1} \sqrt{1 - y_2^2}\,T_y^* K\, dy_2 \tag{14}$$

where $y_1 = y/b$; and y_2 = a variable of integration; K = a scale factor for the arc element dl in terms of y and the angle of inclination β (Grossman 1991), defined by

$$K = \sqrt{\frac{1 - y_1^2 \sin^2\beta}{1 - y_1^2}} \tag{15}$$

From F_x and F_y we may calculate the shear forces (normal to the ellipse) and the tension/compression forces (tangential to the ellipse), F_S and F_T, respectively, at each cross section, as follows:

$$F_T = F_y \sin\gamma - F_x \cos\gamma \tag{16a}$$

$$F_S = F_y \cos\gamma + F_x \sin\gamma \tag{16b}$$

where γ = local slope angle of the elliptical rim, as illustrated in Fig. 2(a). In normalized form

$$F_T^* = F_T/(pb^2); \qquad F_S^* = F_S/(pb^2) \tag{17a,b}$$

With F_S, F_T, and M known at points along the rim, the total strain energy may be found from the formula (Popov 1976)

$$U = \oint \left(\frac{M^2}{2EI} + \frac{F_T^2}{2EA} + \frac{sF_S^2}{2GA}\right) dl \tag{18}$$

where the three terms from left to right represent energy associated with bending, tension/compression, and shear, respectively. Here E and G = moduli of elasticity and shear, respectively, of the rim support material; A = cross section area; I = moment of inertia (for bending) of the cross section; s = a dimensionless factor expressing the fact that the shear stresses are not uniformly distributed over the cross section area, and its value depends on the shape of the cross section. As shown earlier in the load analysis of a rim support without a tension element (Grossman 1991), the shear forces are considerably smaller than the tension/compression forces for typical off-axis geometries; they vanish completely in the rim support of an on-axis membrane.

Eq. (18) may be rewritten in a dimensionless form, by substituting the normalized quantities as follows:

$$U = \frac{p^2 b^7}{EI} \int_{-1}^{+1} (M^{*2} + iF_T^{*2} + jF_S^{*2}) K \, dy_1 \tag{19}$$

where i and j = dimensionless parameters

$$i = \frac{I}{Ab^2} \tag{20}$$

$$j = s \frac{EI}{GAb^2} \tag{21}$$

and are generally much smaller than unity.

F_T^* and F_S^* in (18) are functions of the still unknown F_L^* and P^*; M^* is a function of P^*, F_L^*, and M_L^*. Substitution in (5)–(7) yields

$$\int_{-1}^{+1} M^* \frac{\partial M^*}{\partial M_L^*} K \, dy_1 = 0 \tag{22}$$

$$\int_{-1}^{+1} \left(M^* \frac{\partial M^*}{\partial F_l^*} + iF_T^* \frac{\partial F_T^*}{\partial F_L^*} + jF_S^* \frac{\partial F_S^*}{\partial F_L^*} \right) K \, dy_1 = 0 \tag{23}$$

$$\int_{-1}^{+1} \left(M^* \frac{\partial M^*}{\partial P^*} + iF_T^* \frac{\partial F_T^*}{\partial P^*} + jF_S^* \frac{\partial F_S^*}{\partial P^*} \right) K \, dy_1 = -\left(\frac{EI}{2kb^3} \right) P^* \tag{24}$$

Using (16) and (17) to express F_T^*, F_S^* in terms of F_x^*, F_y^* and calculating the derivatives from (12)–(14), we find

$$\left.\begin{aligned} \partial M^*/\partial M_L^* &= -1;\ \partial M^*/\partial F_L^* = -(1 + y_1);\ \partial M^*/\partial P^* \\ &= (1/2)\sqrt{1 - y_1^2} \cos \beta \\ \partial F_T^*/\partial F_L^* &= \cos \gamma;\ \partial F_S^*/\partial F_L^* = -\sin \gamma \\ \partial F_T^*/\partial P^* &= -(1/2)\sin \gamma\ \partial F_S^*/\partial P^* = -(1/2)\cos \gamma \end{aligned}\right\} \tag{25}$$

and hence (22)–(24) become

$$\int_{-1}^{+1} M^* K \, dy_1 = 0 \tag{26}$$

$$\int_{-1}^{+1} [(1 + y_1)M^* - i \cos \gamma F_T^* + j \sin \gamma F_S^*] K \, dy_1 = 0 \tag{27}$$

$$\int_{-1}^{+1} [\sqrt{1 - y_1^2} \cos \beta M^* - i \sin \gamma F_T^* - j \cos \gamma F_S^*] K \, dy_1 + \left(\frac{EI}{kb^3} \right) P^* = 0 \tag{28}$$

Note that $\sin \gamma$, $\cos \gamma$ in the preceding are functions of y_1 (Grossman 1991)

$$\tan \gamma = \frac{\sqrt{b^2 - y^2}}{y \cos \beta} = \frac{\sqrt{1 - y_1^2}}{y_1 \cos \beta} \tag{29}$$

Let us define

$$H_1(y_1) = \sqrt{1 - y_1^2} \cos \beta \int_{-1}^{y_1} T_y^* K \, dy_2 - (1 + y_1) \int_{-1}^{y_1} T_x^* K \, dy_2 + \int_{-1}^{y_1} [(1 + y_2)T_x^* - \sqrt{1 - y_2^2} \cos \beta T_y^*] K \, dy_2 \tag{30}$$

$$H_2(y_1) = (i \cos^2 \gamma + j \sin^2 \gamma) \int_{-1}^{y_1} T_x^* K \, dy_2 + (j - i) \sin \gamma \cos \gamma \int_{-1}^{y_1} T_y^* K \, dy_2 \tag{31}$$

$$H_3(y_1) = (j \cos^2 \gamma + i \sin^2 \gamma) \int_{-1}^{y_1} T_y^* K \, dy_2 + (j - i) \sin \gamma \cos \gamma \int_{-1}^{y_1} T_x^* K \, dy_2 \tag{32}$$

Then, substitution from (14) in (26) yields

$$M_L^* \int_{-1}^{+1} K \, dy_1 + F_L^* \int_{-1}^{+1} (1 + y_1) K \, dy_1 - \frac{P^*}{2} \cos \beta \int_{-1}^{+1} \sqrt{1 - y_1^2} K \, dy_1 = \int_{-1}^{+1} H_1 K \, dy_1 \tag{33a}$$

Note that in part of the terms in (33*a*), the integrand is antisymmetrical with respect to $y_1 = 0$, which makes the integral from $y_1 = -1$ to $y_1 = +1$ vanish. Hence, (33*a*) may be rewritten in a simplified form

$$(M_L^* + F_L^*) \int_{-1}^{+1} K \, dy_1 - \frac{P^*}{2} \cos \beta \int_{-1}^{+1} \sqrt{1 - y_1^2} K \, dy_1 = \int_{-1}^{+1} H_1 K \, dy_1 \tag{33b}$$

Substitution from (12)–(14) and (16) into (27) gives

$$M_L^* \int_{-1}^{+1} (1 + y_1) K \, dy_1 + F_L^* \int_{-1}^{+1} [(1 + y_1)^2 + i \cos^2 \gamma + j \sin^2 \gamma] K \, dy_1 - \frac{P^*}{2} \int_{-1}^{+1} [(1 + y_1)\sqrt{1 - y_1^2} \cos \beta - (j - i) \sin \gamma \cos \gamma] K \, dy_1 = \int_{-1}^{+1} [(1 + y_1)H_1 - H_2] K \, dy_1 \tag{34a}$$

which may be simplified by eliminating vanishing integrals to give

$$M_L^* \int_{-1}^{+1} K \, dy_1 + F_L^* \int_{-1}^{+1} [(1 + y_1)^2 + i \cos^2 \gamma + j \sin^2 \gamma] K \, dy_1 - \frac{P^*}{2} \cos \beta \int_{-1}^{+1} \sqrt{1 - y_1^2} K \, dy_1 = \int_{-1}^{+1} [(1 - y_1)H_1 - H_2] K \, dy_1 \tag{34b}$$

Finally, substitution from (12)–(14) and (16) into (28) yields

$$M_L^* \cos\beta \int_{-1}^{+1} \sqrt{1 - y_1^2} K\, dy_1$$

$$+ F_L^* \int_{-1}^{+1} [(1 + y_1)\sqrt{1 - y_1^2} \cos\beta - (j - i)\sin\gamma \cos\gamma] K\, dy_1$$

$$- P^* \left(\frac{EI}{kb^3}\right) - \frac{P^*}{2} \int_{-1}^{+1} [(1 - y_1^2)\cos^2\beta + i \sin^2\gamma + j \cos^2\gamma] K\, dy_1$$

$$= \int_{-1}^{-1} [H_3 + H_1\sqrt{1 - y_1^2} \cos\beta] K\, dy_1 \qquad (35a)$$

or, in simplified form

$$(M_L^* + F_L^*)\cos\beta \int_{-1}^{+1} \sqrt{1 - y_1^2} K\, dy_1$$

$$- \frac{P^*}{2} \int_{-1}^{+1} [(1 - y_1^2)\cos^2\beta + i \sin^2\gamma + j \cos^2\gamma] K\, dy_1 - \frac{P^*}{k_1}$$

$$= \int_{-1}^{+1} (H_3 + H_1\sqrt{1 - y_1^2} \cos\beta) K\, dy_1 \qquad (35b)$$

where

$$k_1 = \frac{kb^3}{EI} \qquad (36)$$

Eqs. (33*b*), (34*b*), and (35*b*), provided by Castigliano's second theorem for this statically indeterminate problem, may be solved for F_L^*, M_L^*, and P^*, once the integrals are evaluated. We notice that the integrals contain the membrane loads T_x^*, T_y^*, geometrical parameters of the off-axis paraboloid and rim support, and the cross section parameters, i, j—all given or known from earlier calculations. Also included is the dimensionless parameter k_1 [(36)], which represents the stiffness ratio between the tension element and the rim support. Once the low end reactions F_L^*, M_L^* are found, we can calculate F_H^*, M_H^* from the equilibrium equations (2) and (4), and the entire force and moment distribution from (12)–(14). This completes the problem, since now all the internal forces and moments are given through the expressions already developed, linking them to the low-end reactions.

DEFORMATIONS

A deformation analysis (Grossman 1991) was performed for the off-axis rim support without a tension element. Considering the geometry of the rim support cross section and the elastic properties of its material, the deformations were calculated at all points along the rim based on the loads, forces, and moments found earlier in the load analysis (Grossman 1991). The approach has been to require an accurate elliptical shape for the stressed rim and calculate the corresponding unstressed shape. More specifically, the x- and y-components of the deviation between the unstressed and stressed rim (u and v, respectively) have been expressed in terms of the above parameters. In the notation of the present paper, the relation is as follows:

$$du = \left[2 \sin\left(\frac{\psi + \phi}{2}\right) \sin\left(\frac{\psi - \phi}{2}\right) + \left(\frac{pb^2}{EA}\right) F_T^* \cos\phi\right] \cdot \sqrt{\frac{1 - y_1^2 \sin^2\beta}{1 - y_1^2}} \frac{dy}{c} \qquad (37)$$

$$dv = \left[-2 \cos\left(\frac{\psi + \phi}{2}\right) \sin\left(\frac{\psi - \phi}{2}\right) + \left(\frac{pb^2}{EA}\right) F_T^* \sin\phi\right] \cdot \sqrt{\frac{1 - y_1^2 \sin^2\beta}{1 - y_1^2}} \frac{dy}{c} \qquad (38)$$

where

$$c = 1 + \frac{F_T}{EA} = 1 + \left(\frac{pb^2}{EA}\right) F_T^* \qquad (39)$$

and

$$\psi \pm \phi = \int_{-1}^{y_1} \left[\frac{\cos\beta}{(1 - y_2^2 \sin^2\beta)^{3/2}} (1 + c) - \left(\frac{pb^4}{EI}\right) \frac{M^*}{c}\right] \sqrt{\frac{1 - y_2^2 \sin^2\beta}{1 - y_2^2}} \frac{dy_2}{c} \qquad (40)$$

The same deformation analysis may be applied to the present case, with a tension element. However, the loads M^* and F_T^* in (37)–(40) must be replaced by those calculated under the present conditions, (14) and (17), with proper consideration for the effect of the string force P. The procedure for doing so has been incorporated in a computer code that calculates loads and deformations in the off-axis rim support.

RESULTS AND COMMENT

The computer code, described in the earlier load and deformation analyses (Grossman 1991), has been modified to include the option of a tension element along the major axis of the elliptical rim. The code calculates numerically the elliptical integrals contained in the mathematical results of the foregoing analysis and evaluates the loads and deformations at user-specified points along the rim. To use the code for a case with a tension element, the user must specify a nonzero value of the parameter $k_1 = (kb^3/EI)$, (36). As an example for the discussion, calculations were carried out for the geometry of the Deployable Solar Concentrator (Grossman and Williams 1989, 1990), with the parameters given in (1). We have assumed $i = j = 0$, a good assumption for most practical cases.

Grossman (1991) showed that the dominant factor in the strength requirements for an off-axis rim support are the bending moments. Fig. 3 shows the distribution of the moments along the rim for two cases: on the left is the distribution for the case without a tension element; on the right are the moments of the same rim support with an added tension element of relative stiffness $k_1 = 1{,}000$. It is evident from Fig. 3 that the tension element contributes to a major reduction in the moments all over the rim. The maximum moment is reduced from $0.2111pb^3$ to $0.0927pb^3$. Under the given conditions, the location of the maximum moment changes from the

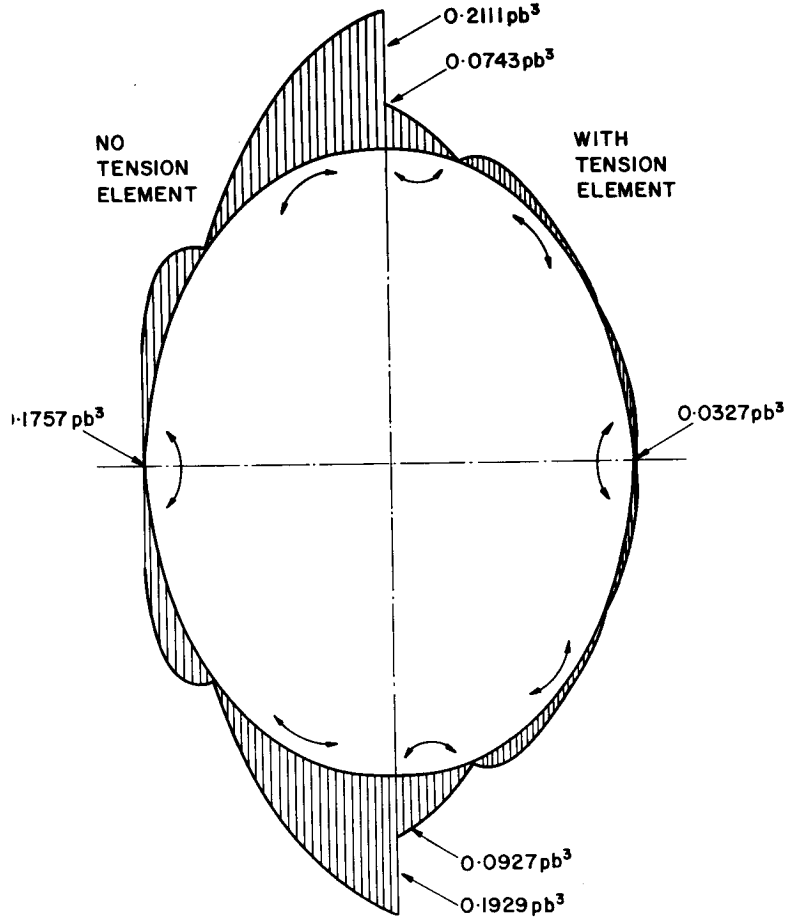

FIG. 3. Distribution along Rim of Internal Moments with and without Tension Element

top to the bottom of the ellipse. Without a tension element, the moment reverses direction twice, tending to increase the ovality of the ellipse. The tension element attempts to fix the distance along the major axis, thereby causing the moment to change direction four times, as shown.

The effectiveness of the tension element in reducing the moments depends on its stiffness relative to that of the rim support. Fig. 4 shows the dimensionless bending moments (dashed lines), as functions of $k_1 = (kb^3/EI)$ at three points along the rim: M_L^* at $(0, -b)$, M_0^* at $(b \cos \beta, 0)$, and M_H^* at $(0, +b)$. Also shown is the dimensionless tension force (solid line) $P^* = (P/pb^2)$ in the element. It is evident that all three moments decrease in absolute magnitude and the element force increases as the relative rigidity increases. At about $k_1 = 10$, M_L^*, and M_H^* reverse direction due to the effect explained earlier. At about $k_1 = 1{,}000$, all three moments approach an asymptotic value. It seems desirable to select a design point at k_1 values greater than 1,000, where the sensitivity to k_1 is minimal.

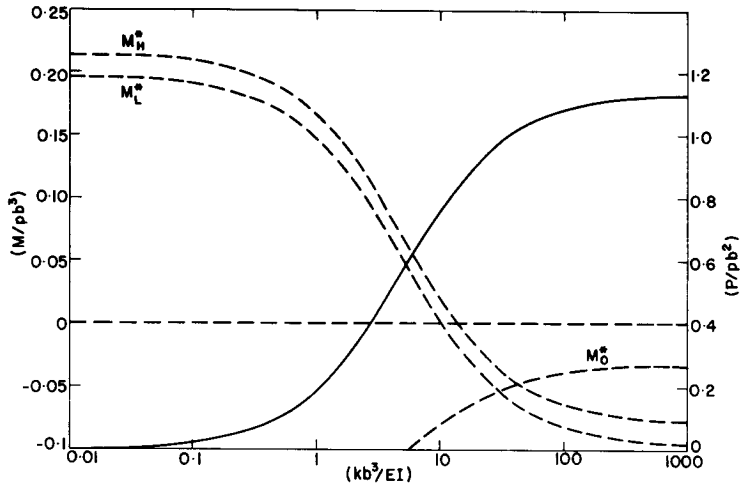

FIG. 4. Dimensionless Bending Moments and Tension Force as Functions of Tension Element Stiffness

How can such element stiffness be achieved? For the Deployable Solar Concentrator (Grossman and Williams 1989, 1990), a 1-m diameter, 9 × 7-m inflatable torus made of 0.007 in. (1.8×10^{-4} m) thick neoprene-coated woven Kevlar fabric has been designed; the material modulus of elasticity is $E = 500{,}000$ psi (3.4×10^6 kPa), and the cross-sectional moment of inertia is $I = 176$ in.^{4} (7.07×10^{-6} m^4). To obtain $k_1 = 1{,}000$ with $b = 180$ in. (4.57 m) the spring constant for the tension element must be 15,000 lbf/in. (2.7×10^6 N/m). This may be achieved with a 0.6-mm diameter woven Kevlar string of 19,000,000 psi (1.3×10^8 kPa) modulus.

The tension element is effective in reducing not only the loads but also the deformations. Fig. 5 describes the stressed shape (solid line) and the unstressed shape (broken line) of the rim support for the Deployable Solar Concentrator (Grossman and Williams 1989, 1990) geometry. The deformation in Fig. 5 is not to scale and has been exaggerated for better illustration. Assuming the point $(0, -b)$ to be common for the stressed and unstressed rim, the drawing shows the maximum y deformation (v_{max}) at the $(0, +b)$ location and the maximum x deformation (u_{max}) at the $(b \cos \beta, 0)$ location. For the 9 × 7 m, 40 in. diameter inflatable torus, the deformation-governing rigidity parameter (Grossman 1991), (pb^4/EI) is approximately 0.03. With this value and without a tension element the calculations show $u_{max} = 0.0017b$ and $v_{max} = 0.0025b$. Adding a tension element with relative stiffness $k_1 = 1{,}000$ reduces both those deformations to below $0.0001b$.

CONCLUSION

Earlier load and deformation analyses by Grossman (1991) of an off-axis rim support were extended to include the effect of a tension element added along the major axis of the ellipse. Such an element, in the form of a string or cable, restrains the tendency for increased ovality of the rim support under load without seriously interfering with the packaging and deployment of the device, at negligible added mass. The analysis has shown that a

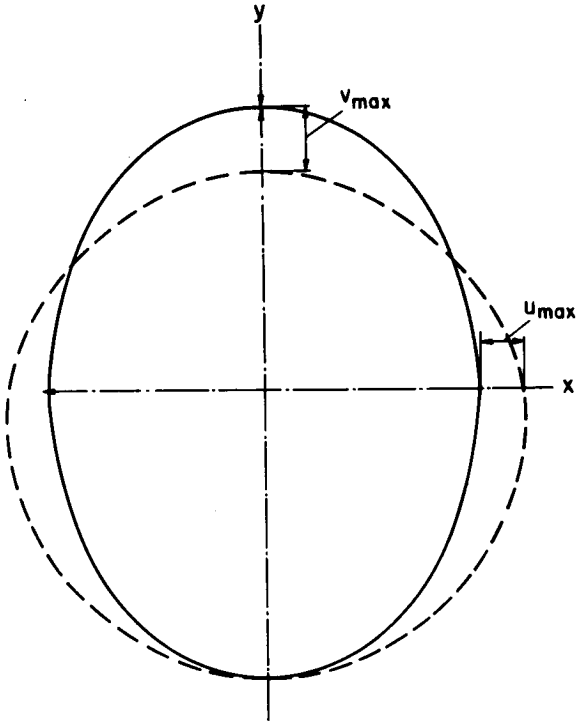

FIG. 5. Stressed and Unstressed Shape of Rim Support with Tension Element for Geometry of Deployable Solar Concentrator (Grossman and Williams 1989, 1990)

properly designed tension element can reduce the maximum bending moment by more than a factor of 2 for the Deployable Solar Concentrator (Grossman and Williams 1989, 1990) geometry. The deformations are reduced by more than a factor of 20. To achieve asymptotic reduction of loads, the stiffness of the tension element relative to that of the rim support, as expressed by the dimensionless parameter $k_1 = (pb^3/EI)$, must exceed 1,000.

ACKNOWLEDGMENT

This study was conducted under USAF/AFAL Contract F04611-86-C-0112.

APPENDIX I. REFERENCES

Grossman, G. (1991). "Analysis of rim supports for off-axis inflatable reflectors. Part I: Loads." *J. Aerosp. Engrg.*, ASCE, 4(1), 47–66.
Grossman, G. (1991). "Analysis of rim supports for off-axis inflatable reflectors. Part II: Deformations." *J. Aerosp. Engrg.*, ASCE, 4(1), 67–77.
Grossman, G., and Williams, G. (1990). "Inflatable concentrators for solar propulsion and dynamic space power." *Trans. ASME, J. Solar Energy Engrg.*, 112, 229–236.
Grossman, G., and Williams, G. (1989). "Inflatable concentrators for solar propulsion and dynamic space power." *Proc., 1989 Int. Solar Energy Conf.*, San Diego, Calif., 39–45.

Marin, J., and Sauer, J. A. (1954). *Strength of materials*. The Macmillan Co., New York, N.Y., 238–269.
Popov, E. P. (1976). *Mechanics of materials*. Prentice-Hall, Inc., Englewood Cliffs, N.J., 525–556.
Williams, G. (1987). "Inflatables for lightweight satellite applications." *1st Annu. USU Conf. on Small Satellites*, Logan, Utah.

APPENDIX II. NOTATION

The following symbols are used in this paper:

A = cross-section area (m^2);
b = half major axis of elliptical rim (m);
c = dimensionless parameter, (39);
E = modulus of elasticity (N/m^2);
F = focal length of on-axis, parent paraboloid (m);
F_H = compression/tension force at high-cut end of rim, Fig. 2 (N);
F_H^* = F_H/pb^2 (dimensionless);
F_L = compression/tension force at low-cut end of rim, Fig. 2 (N);
F_L^* = F_L/pb^2 (dimensionless);
F_S = shear force in rim (N);
F_S^* = F_S/pb^2 (dimensionless);
F_T = compression/tension force in rim (N);
F_T^* = F_T/pb^2 (dimensionless);
F_x = internal force in x-direction, Fig. 2 (N);
F_x^* = F_x/pb^2 (dimensionless);
F_y = internal force in y-direction, Fig. 2 (N);
F_y^* = F_y/pb^2 (dimensionless);
G = shear modulus (N/m^2);
H_1 = dimensionless parameter, (30);
H_2 = dimensionless parameter, (31);
H_3 = dimensionless parameter, (32);
I = moment of inertia of cross section (m^4);
i = I/Ab^2 (dimensionless);
j = sEI/GAb^2 (dimensionless);
K = dimensionless parameter, (15);
k = spring constant of tensions element (N/m);
k_1 = relative stiffness of tension element (kb^3/EI) (dimensionless);
l = arc length along rim (m);
M = internal moment, Fig. 2 (N·m);
M^* = M/pb^3 (dimensionless);
M_H = internal moment at high-cut end of rim, Fig. 2, (N·m);
M_H^* = M_H/pb^3 (dimensionless);
M_L = internal moment at low-cut end of rim, Fig. 2 (N·m);
M_L^* = M_L/pb^3 (dimensionless);
P = tension force in tension element (N);
P^* = dimensionless force in tension element (P/pb^2) (dimensionless);
p = inflation pressure (N/m^2);
s = factor in (18), expressing the nonuniform distribution of shear stresses over cross section (dimensionless);
T_x = tensile force exerted by membrane on rim support in the x-direction (N/m);

T_x^* = T_x/pb (dimensionless);
T_y = tensile force exerted by membrane on rim support in y-direction (N/m);
T_y^* = T_y/pb (dimensionless);
U = strain energy, (18) (J);
u = deformation in x-direction (m);
v = deformation in y-direction (m);
x = rim coordinate along minor axis (m);
y = rim coordinate along major axis (m);
y_1 = y/b (dimensionless);
y_2 = variable of integration for y_1 (dimensionless);
β = angle of inclination of the off-axis rim (rad);
γ = slope angle of elliptical rim, (29) (rad);
δ = elongation of tension element (m);
ϕ = dimensionless parameter, (40); and
ψ = dimensionless parameter, (40).

L•Garde Inc
15181 Woodlawn Avenue
Tustin, CA 92780-6487
www.LGarde.com